

# Spin-orbital frustrations and anomalous metallic state in iron-pnictide superconductors

Frank Krüger,<sup>1</sup> Sanjeev Kumar,<sup>2,3</sup> Jan Zaanen,<sup>2</sup> and Jeroen van den Brink<sup>2,4</sup>

<sup>1</sup>*Department of Physics, University of Illinois, 1110 West Green Street, Urbana, Illinois 61801, USA*

<sup>2</sup>*Instituut-Lorentz, Universiteit Leiden, P.O. Box 9506, 2300 RA Leiden, The Netherlands*

<sup>3</sup>*Faculty of Science and Technology, University of Twente, P.O. Box 217, 7500 AE Enschede, The Netherlands*

<sup>4</sup>*Institute for Molecules and Materials, Radboud Universiteit Nijmegen, P.O. Box 9010, 6500 GL Nijmegen, The Netherlands*

(Received 25 November 2008; published 6 February 2009)

We develop an understanding of the anomalous metal state of the parent compounds of recently discovered iron-based superconductors starting from a strong-coupling viewpoint, including orbital degrees of freedom. On the basis of an intermediate-spin ( $S=1$ ) state for the  $\text{Fe}^{2+}$  ions, we derive a Kugel-Khomskii spin-orbital Hamiltonian for the active  $t_{2g}$  orbitals. It turns out to be a highly complex model with frustrated spin and orbital interactions. We compute its classical phase diagrams and provide an understanding for the stability of the various phases by investigating its spin-only and orbital-only limits. The experimentally observed spin-stripe state is found to be stable over a wide regime of physical parameters and can be accompanied by three different types of orbital orders. Of these the orbital-ferro and orbital-stripe orders are particularly interesting since they break the in-plane lattice symmetry—a robust feature of the undoped compounds. We compute the magnetic excitation spectra for the effective spin Hamiltonian, observing a strong reduction in the ordered moment, and point out that the proposed orbital ordering pattern can be measured in resonant x-ray diffraction.

DOI: [10.1103/PhysRevB.79.054504](https://doi.org/10.1103/PhysRevB.79.054504)

PACS number(s): 74.25.Jb, 74.70.-b, 74.20.Mn, 74.25.Ha

## I. INTRODUCTION

The beginning of this year marked the discovery of a new and very unusual family of high-temperature superconductors: the iron pnictides. Superconductivity at 26 K was discovered in fluorine-doped rare-earth iron oxypnictide  $\text{LaOFeAs}$ .<sup>1,2</sup> In subsequent experimental studies involving different rare-earth elements a superconducting  $T_c$  larger than 50 K was reported.<sup>3–5</sup> Since then a large number of experimental and theoretical papers have been published, making evident the immense interest of the condensed-matter community in this subject.<sup>6</sup>

It has become clear that the iron-pnictide superconductors have, besides a number of substantial differences, at least one striking similarity with the copper oxides: the superconductivity emerges by doping an antiferromagnetic (AF) non-superconducting parent compound. This antiferromagnetism is however of a very unusual kind. Instead of the simple staggered  $(\pi, \pi)$  antiferromagnetism of the undoped cuprates, this “stripe” or  $(\pi, 0)$  spin order involves rows of parallel spins on the square Fe-ion lattice that are mutually staggered.<sup>7</sup> In fact, before this order sets in a structural phase transition occurs where the two in-plane lattice constants become inequivalent. This structural distortion is very small, but it appears that the electron system undergoes a major reorganization at this transition. This is manifested by resistivity anomalies, drastic changes in the Hall and Seebeck coefficients, and so on.<sup>8</sup> Although the magnetic and structural distortions appear to be coincident in the 122 family,<sup>7,9</sup> in the 1111 compounds they are clearly separated,<sup>7</sup> and there it is obvious that the large scale changes in the electron system occur at the structural transition, while barely anything is seen at the magnetic transition.

Given that the structural deformation is minute, this is an apparent paradox. Assuming that only the spins matter one could envisage that the spin ordering would lead to a drastic

nesting-type reorganization of the Fermi surfaces, causing a strong change in the electronic properties. But why is there so little happening at the magnetic transition? One could speculate that the spins are fluctuating in fanciful ways and that these fluctuations react strongly to the structural change.<sup>10–12</sup> Such possibilities cannot be excluded on theoretical grounds but whichever way one wants to proceed invoking only spins and itinerant carriers: one is facing a problem of principle.

This paper is dedicated to the cause that valuable lessons can be learned from the experiences with manganites when dealing with the pnictides. A crucial lesson learned over a decade ago, when dealing with the colossal magnetoresistance (CMR) physics of the manganites, was the demonstration by Millis *et al.*<sup>13</sup> that the coupling between fluctuating spins and charge carriers can only cause relatively weak transport anomalies. In the pnictides one finds that the resistivity drops by a couple of  $\text{m}\Omega \text{ cm}$ , that the Hall mobility increases by 2–3 orders of magnitude, and most significantly the Seebeck coefficient drops by an order of magnitude from a high-temperature limit order value of  $40 \mu\text{V/K}$  in crossing the transition. It is very questionable if spin-carrier coupling of any kind, be it itinerant or strongly coupled, can explain such large changes in the transport properties.

### A. Role of electron-electron interactions

Comparing the pnictides with the cuprate superconductors there is now a consensus that in two regards these systems are clearly different: (i) in the pnictide system no Mott insulator has been identified indicating that they are “less strongly correlated” than the cuprates in the sense of the Hubbard-type local interactions; and (ii) in the pnictide one has to account for the presence of several  $3d$  orbitals playing a role in the low-energy physics, contrasting with the single  $3d_{x^2-y^2}$  orbital that is relevant in the cuprates.

As a consequence, the prevailing viewpoint is to regard the pnictides as local-density approximation (LDA) metals, where the multiorbital nature of the electronic structure gives rise to a multisheeted Fermi surface, while the “correlation effects” are just perturbative corrections, causing moderate mass enhancements and so on.

Although there is evidence that the system eventually discovers this “Fermi-liquid fixed point” at sufficiently low temperatures, it is hard to see how this can explain the properties of the metallic state at higher temperatures. The data alluded to in the above indicate pronounced “bad metal” behavior, and these bad metal characteristics do not disappear with doping. In fact, one can argue that the term bad metal actually refers to a state of ignorance: it implies that the electron system cannot possibly be a simple coherent Fermi liquid.

### B. Spin-charge-orbital correlations

Another important lesson from the manganites is that the presence of multiple orbitals can mean much more than just the presence of multiple LDA bands at the Fermi energy. Also in iron pnictides orbital degree of freedom can become relevant.<sup>14</sup> Manganite *metals* have a degree of itineracy in common with the pnictides, but they still exhibit correlated electron physics tied to orbital degeneracy which is far beyond the reach of standard band-structure theory.

The seminal work by Kugel and Khomskii (KK) (Ref. 15) in the 1970s made clear that in Mott insulators orbital degrees of freedom turn into dynamical spinlike entities that are capable of spinlike ordering phenomena under the condition that in the local limit one has a Jahn-Teller (orbital) degeneracy. The resulting orbital degrees of freedom can have in dynamical regards a “life of their own.” This manifests itself typically in transitions characterized by small changes in the lattice accompanied by drastic changes in the electronic properties.

In the manganites there are numerous vivid examples of the workings of orbital ordering.<sup>16–18</sup> Under the right circumstances one can find a transition from a high-temperature cubic phase to a low-temperature tetragonal phase accompanied by a quite moderate change in the lattice but with a change in the electron system that is as drastic as a “dimensional transmutation.” This system changes from an isotropic three-dimensional (3D) metal at high temperature to a quasi-two-dimensional electron system at low temperatures where the in-plane resistivity is orders of magnitude lower than the  $c$ -axis resistivity.<sup>19–21</sup>

The explanation is that one is dealing in the cubic manganite with a  $\text{Mn}^{3+}$  ion with an  $e_g$  Jahn-Teller degeneracy involving  $3d_{x^2-y^2}$  and  $3d_{3z^2-1}$  orbitals. In the low-temperature “A phase” one finds a ferro-orbital order where cooperatively the  $x^2-y^2$  orbitals are occupied. This greatly facilitates the hopping in the planes, while for simple orthogonality reasons coherent transport along the  $c$  axis is blocked. Since the  $d$  electrons only contribute modestly to the cohesive energy of the crystal, this large scale change in the low-energy degrees of freedom of the electronic system reflect only barely in the properties of the lattice. On the other hand, this orbital order

is a necessary condition for the spin system to order, and at a lower temperature one finds a transition to a simple staggered antiferromagnet, in tune with the observation that in the A phase the effective microscopic electronic structure is quite similar to the ones found in cuprate planes.

The ruthenates are another class of materials in which the orbital degrees of freedom play a decisive role, in both the metallic and insulating phases. Bilayer  $\text{Ca}_3\text{Ru}_2\text{O}_7$ , for instance, has attracted considerable interest because the observed CMR effect is possibly driven by orbital scattering processes among the conduction electrons.<sup>22,23</sup> Another example is  $\text{Ti}_2\text{Ru}_2\text{O}_7$ , in which below 120 K its 3D metallic state shows a dramatic dimensional reduction and freezes into a quasi-one-dimensional spin system, accompanied by a fundamental orbital reorganization.<sup>24,25</sup>

It is very remarkable that the ground state of all iron pnictides is characterized by a very similar spatial anisotropy of the magnetic exchange interactions: along one direction in the plane the Fe-Fe bonds are strong and antiferromagnetic, whereas in the orthogonal direction they are very weak and possibly even ferromagnetic.<sup>26</sup> With all the others, also this observation is consistent with our hypothesis that the undoped iron pnictides are controlled by “spin-charge-orbital” physics, very similar to the ruthenates and manganites.

### C. Organization of this paper

In Sec. II of this paper we derive the spin-orbital Hamiltonian starting with a three-orbital Hubbard model for the iron square lattice of the iron pnictides. The phase diagrams in the classical limit of this Hamiltonian are discussed in Sec. III. We analyze the various phase transitions by also considering the corresponding spin-only and orbital-only models. Section IV deals with the results on magnetic excitation spectra, which provide a possible explanation for the reduction in magnetic moment, a central puzzle in the iron superconductors. We conclude by commenting briefly on how the itineracy may go hand in hand with the orbital “tweed” order that we put forward in the present study and point out that the tweed orbital ordered state can, in principle, be observed in resonant x-ray diffraction experiments.

## II. SPIN-ORBITAL MODEL FOR IRON PLANES

As stated above, the superconducting iron pnictides are not strongly coupled doped Mott insulators. Staying within the realm of Hubbard-model language they are likely to be in the intermediate coupling regime where the Hubbard  $U$ 's are of order of the bandwidth. To at least develop qualitative insight in the underlying physics it is usually a good idea to approach this regime from strong coupling for the simple reason that more is going on in strong-coupling band than in the weak-coupling band-structure limit. As the experience with for instance the manganites and ruthenates shows, this is even more true when we are dealing with the physics associated with orbital degeneracy. The orbital ordering phenomena that we have already alluded to take place in itinerant systems but their logic is quite comprehensible starting from the strongly coupled side.

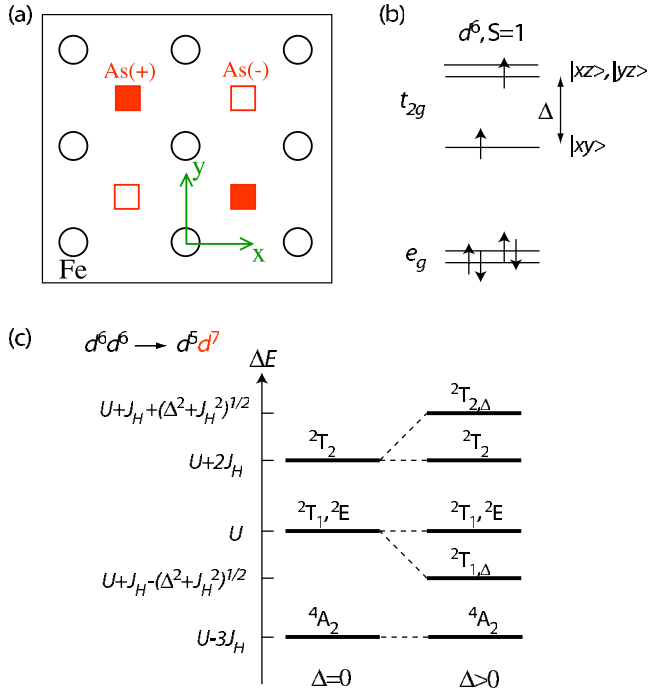


FIG. 1. (Color online) (a) Fe square lattice (circles) and relative positions of the As ions. The latter are located in adjacent layers above (filled squares) and below (empty squares) the Fe plaquettes. (b) Schematic illustration of a ground-state  $d^6$  configuration of the Fe ions corresponding to an intermediate  $S=1$  spin state. (c) Multiplet structure of the  $d_i^6 d_j^6 \Rightarrow d_i^5 d_j^7$  charge excitations for localized  $e_g$  electrons.

Thus as a first step we will derive the spin-orbital model of pnictides starting from a localized electron framework. A condition for orbital phenomena to occur is then that the crystal fields conspire to stabilize an intermediate spin ( $S=1$ ) ionic states. These crystal fields come in two natural varieties: one associated with the tetrahedral coordination of Fe by the As atoms, and a tetragonal field associated with the fact that the overall crystal structure consists of layers. When these crystal fields would be both very large the Fe  $3d^6$  ions would form a low-spin singlet state. This is excluded by the observation of magnetism, and moreover band-structure calculations indicate that the crystal fields are relatively small.

The other extreme would be the total domination of Hund's rule couplings, and this would result in a high-spin  $S=2$  state, which appears to be the outcome of spin-polarized LDA and LDA+ $U$  calculations.<sup>27</sup> However, given that for elementary chemistry reasons one expects that the tetrahedral splitting is much larger than the tetragonal splitting, there is the possibility that Hund's rule overwhelms the latter but loses from the former, resulting in an "intermediate"  $S=1$  state. Although the issue is difficult to decide on microscopic grounds, for orbital physics to be relevant we need an intermediate spin state as in the present crystal-field scheme this is the only ionic  $d^6$  state that exhibits a Jahn-Teller ground-state degeneracy (see Fig. 1).

In this situation the starting Hubbard model involves a nondegenerate  $|xy\rangle$  and two doubly-degenerate,  $|xz\rangle$  and  $|yz\rangle$ , orbitals, as will be defined in Sec. II A. The details of the derivation of the model are given in Sec. II B. The derivation

does not assume any specific structure for the hopping parameters and, hence, is completely general. The algebra involved in the derivation is tedious but straightforward and a general reader may wish to skip Sec. II B and jump directly to Sec. II C where we discuss the relevant hopping processes for the Fe-As plane. Incorporating these hopping parameters leads to the model relevant to the iron plane.

### A. Hubbard model for pnictide planes for the intermediate spin $d^6$ state

The iron ions are in a  $d^6$  configuration where we assume the low-lying  $e_g$  orbitals to be fully occupied due to a large crystal-field splitting between the  $e_g$  and  $t_{2g}$  states. The two remaining electrons occupy the three  $t_{2g}$  orbitals  $|a\rangle := |xz\rangle$ ,  $|b\rangle := |yz\rangle$ , and  $|c\rangle := |xy\rangle$  with  $x$  and  $y$  pointing along the bonds of the iron square lattice. Due to Hund's coupling  $J_H$  between the  $t_{2g}$  electrons, such a configuration leads to an  $S=1$  intermediate spin state of the  $d^6$  Fe ions. Further, we incorporate a small tetragonal splitting  $\Delta$  between the  $|xy\rangle$  state and the  $|xz\rangle, |yz\rangle$  doublet (see Fig. 1).

Assuming the  $e_g$  electrons to be localized, the physical situation is very similar to almost cubic vanadates such as  $YVO_3$  or  $LaVO_3$  where the two  $d$  electrons of the  $V^{3+}$  ions occupy nearly degenerate  $t_{2g}$  orbitals. Interestingly, in these systems orbital ordering in the presence of a small crystal-field splitting  $\Delta$  can lead to C-type antiferromagnetism<sup>28-30</sup> characterized by an ordering wave vector  $\mathbf{Q} = (\pi, \pi, 0)$ . The effective Hubbard model for the  $t_{2g}$  electrons consists of a kinetic-energy part  $\mathcal{H}_t$ , a crystal-field splitting  $\mathcal{H}_{cf}$ , and of the on-site electron-electron interactions  $\mathcal{H}_{int}$ ,

$$\mathcal{H} = \mathcal{H}_t + \mathcal{H}_{cf} + \mathcal{H}_{int}, \quad (1)$$

with a kinetic-energy contribution that is much richer than in the vanadates. For the nearest-neighbor bonds the effective hoppings between the Fe  $t_{2g}$  orbitals have contributions from both direct  $d-d$  and  $d-p-d$  processes via As  $p$  orbitals. These As ions are located in adjacent layers above or below the Fe ion plaquettes as illustrated in Fig. 1(a). Because of this particular geometry, the indirect As-mediated hoppings should be of similar strength for nearest-neighbor and next-nearest-neighbor Fe ions. At this point, we do not specify the effective hopping matrix elements  $t_{\alpha\beta}^{(i,j)}$  between orbitals  $\alpha, \beta = a, b, c$  along a particular bond  $(i, j)$  and write the kinetic-energy operator in the most general form,

$$\mathcal{H}_t = - \sum_{(i,j)} \sum_{\alpha\beta\sigma} t_{\alpha\beta}^{(i,j)} (d_{i\alpha\sigma}^\dagger d_{j\beta\sigma} + \text{H.c.}), \quad (2)$$

where  $d_{i\alpha\sigma}^\dagger$  ( $d_{i\alpha\sigma}$ ) creates (annihilates) an electron on site  $i$  in orbital  $\alpha$  with spin  $\sigma = \uparrow, \downarrow$ . The crystal-field splitting between the  $t_{2g}$  orbitals is simply given by

$$\mathcal{H}_{cf} = \sum_{i\alpha} \epsilon_\alpha \hat{n}_{i\alpha}, \quad (3)$$

with  $\hat{n}_{i\alpha} = \sum_\sigma \hat{n}_{i\alpha\sigma}$  and  $\hat{n}_{i\alpha\sigma} = d_{i\alpha\sigma}^\dagger d_{i\alpha\sigma}$ . In our case the electron energies are given by  $\epsilon_c = 0$  for the  $xy$  and  $\epsilon_a = \epsilon_b = \Delta$  for the  $xz$  and  $yz$  orbitals. The electron-electron interactions are described by the on-site terms,<sup>31</sup>

$$\begin{aligned} \mathcal{H}_{\text{int}} = & U \sum_{i\alpha} \hat{n}_{i\alpha\uparrow} \hat{n}_{i\alpha\downarrow} + \frac{1}{2} \left( U - \frac{5}{2} J_H \right) \sum_{i\alpha\beta}^{\alpha \neq \beta} \hat{n}_{i\alpha} \hat{n}_{i\beta} \\ & + J_H \sum_{i\alpha\beta}^{\alpha \neq \beta} d_{i\alpha\uparrow}^\dagger d_{i\alpha\downarrow}^\dagger d_{i\beta\downarrow} d_{i\beta\uparrow} - J_H \sum_{i\alpha\beta}^{\alpha \neq \beta} \hat{S}_{i\alpha} \hat{S}_{i\beta}, \quad (4) \end{aligned}$$

with the Coulomb element  $U$  and a Hund's exchange element  $J_H$ .

### B. Superexchange model

In the limit of strong Coulomb repulsion,  $t \ll U$ , charge fluctuations  $d_i^\dagger d_j^\dagger \Rightarrow d_i^\dagger d_j^\dagger$  are suppressed and on each site the two  $t_{2g}$  electrons have to form a state belonging to the ground-state manifold of  $\mathcal{H}_{\text{int}} + \mathcal{H}_{\text{cf}}$  in the two-electron sector. For sufficiently small crystal-field splitting,  $\Delta^2 < 8J_H^2$ , these states are given by two  $S=1$  triplets in which on each site either the  $xz$  or  $yz$  is unoccupied. This orbital degree of freedom can be viewed as a  $T=\frac{1}{2}$  pseudospin. From Eqs. (3) and (4) we easily obtain  $E_0 = U - 3J_H + \Delta$  as the ground-state energy of the  $t_{2g}^2$  sector.

A general spin-orbital superexchange model can be derived by second-order perturbation theory controlled by the kinetic-energy contribution  $\mathcal{H}_t$ , where we have to consider all virtual processes  $t_{2g}^2 t_{2g}^2 \rightarrow t_{2g}^1 t_{2g}^3 \rightarrow t_{2g}^2 t_{2g}^2$  acting on the  $S=1$  and  $T=1/2$  ground-state manifolds. The most general superexchange Hamiltonian in the sense of Kugel and Khomskii for a given bond  $(i, j)$  takes the form,

$$\mathcal{H}_{\text{KK}}^{(i,j)} = - \sum_{\tau_i, \tau_j} \sum_{s_i, s_j} J_{\tau_i, \tau_j, s_i, s_j}^{(i,j)} A_{\tau_i, \tau_j}^{(i,j)} (\hat{T}_i, \hat{T}_j) \times B_{s_i, s_j} (\hat{S}_i, \hat{S}_j), \quad (5)$$

where  $\hat{S}$  and  $\hat{T}$  denote the spin  $S=1$  and pseudospin  $T=\frac{1}{2}$  operators. The functional form of  $B$  only depends on total spins  $s_i$  and  $s_j$  on the two sites in the intermediate  $t_{2g}^1 t_{2g}^3$  states. Whereas the single-occupied site has necessarily  $s=1/2$ , the other site can be in a high-spin ( $s=3/2$ ) or low-spin ( $s=1/2$ ) state. Likewise, the functions  $A^{(i,j)}$  are determined by the pseudospins,  $\tau_i$  and  $\tau_j$ , of the involved intermediate states.

To derive the effective spin-orbital superexchange model we have to find the multiplet structure of the virtual intermediate  $t_{2g}^3$  configurations. It is straightforward to diagonalize  $\mathcal{H}_{\text{cf}} + \mathcal{H}_{\text{int}}$  in Eqs. (3) and (4) in the three-particle sector. The lowest energy we find for the  ${}^4A_2$  quartet of  $s=3/2$  high-spin intermediate states

$$\left| {}^4A_2, \frac{3}{2}, s^z \right\rangle,$$

with

$$\left| s^z \right\rangle = \left| \frac{3}{2} \right\rangle = d_{a\uparrow}^\dagger d_{b\uparrow}^\dagger d_{c\uparrow}^\dagger |0\rangle,$$

$$\left| \frac{1}{2} \right\rangle = \frac{1}{\sqrt{3}} (d_{a\uparrow}^\dagger d_{b\uparrow}^\dagger d_{c\downarrow}^\dagger + d_{a\uparrow}^\dagger d_{b\downarrow}^\dagger d_{c\uparrow}^\dagger + d_{a\downarrow}^\dagger d_{b\uparrow}^\dagger d_{c\uparrow}^\dagger) |0\rangle,$$

$$\left| -\frac{1}{2} \right\rangle = \frac{1}{\sqrt{3}} (d_{a\downarrow}^\dagger d_{b\downarrow}^\dagger d_{c\uparrow}^\dagger + d_{a\downarrow}^\dagger d_{b\uparrow}^\dagger d_{c\downarrow}^\dagger + d_{a\uparrow}^\dagger d_{b\downarrow}^\dagger d_{c\downarrow}^\dagger) |0\rangle,$$

and

$$\left| -\frac{3}{2} \right\rangle = d_{a\downarrow}^\dagger d_{b\downarrow}^\dagger d_{c\downarrow}^\dagger |0\rangle.$$

Their energy is  $\epsilon({}^4A_2) = E({}^4A_2) - 2E_0 = U - 3J_H$ , where  $E_0 = U - 3J_H + \Delta$  is the ground-state energy in the  $t_{2g}^2$  sector. In order for the approach to be valid we have to assume that the system has a charge-transfer gap,  $U - 3J_H > 0$  and that the hopping matrix elements are sufficiently small compared to the charge-transfer gap. All the other multiplets consist of intermediate  $s=1/2$  doublets. The  ${}^2E$  multiplet with excitation energy  $\epsilon({}^2E) = U$  consist of the two spin- $\frac{1}{2}$  doublets,

$$\left| {}^2E, \frac{1}{2}, \sigma \right\rangle_1 = \frac{1}{\sqrt{6}} (2d_{a\sigma}^\dagger d_{b\sigma}^\dagger d_{c,-\sigma}^\dagger - d_{a\sigma}^\dagger d_{b,-\sigma}^\dagger d_{c,\sigma}^\dagger - d_{a,-\sigma}^\dagger d_{b\sigma}^\dagger d_{c\sigma}^\dagger) |0\rangle, \quad (6)$$

$$\left| {}^2E, \frac{1}{2}, \sigma \right\rangle_2 = \frac{1}{\sqrt{2}} (d_{a,-\sigma}^\dagger d_{b\sigma}^\dagger d_{c\sigma}^\dagger - d_{a\sigma}^\dagger d_{b,-\sigma}^\dagger d_{c\sigma}^\dagger) |0\rangle. \quad (7)$$

Finally, we have multiplets  ${}^2T_1^{(\Delta)}$  and  ${}^2T_2^{(\Delta)}$  which consist of spin- $\frac{1}{2}$  doublets and invoke doubly-occupied orbitals,

$$\left| {}^2T_{1/2}, \frac{1}{2}, \sigma \right\rangle = \frac{1}{\sqrt{2}} d_{c\sigma}^\dagger (d_{a\uparrow}^\dagger d_{a\downarrow}^\dagger \mp d_{b\uparrow}^\dagger d_{b\downarrow}^\dagger) |0\rangle, \quad (8)$$

with excitation energies  $\epsilon({}^2T_1) = U$  and  $\epsilon({}^2T_2) = U + 2J_H$ , and

$$\left| {}^2T_{1/2}^\Delta, \frac{1}{2}, \sigma \right\rangle_1 = d_{a\sigma}^\dagger (\sqrt{1 - v_\mp^2} d_{c\uparrow}^\dagger d_{c\downarrow}^\dagger \mp v_\mp d_{a\uparrow}^\dagger d_{a\downarrow}^\dagger) |0\rangle, \quad (9)$$

$$\left| {}^2T_{1/2}^\Delta, \frac{1}{2}, \sigma \right\rangle_2 = d_{b\sigma}^\dagger (\sqrt{1 - v_\mp^2} d_{c\uparrow}^\dagger d_{c\downarrow}^\dagger \mp v_\mp d_{b\uparrow}^\dagger d_{b\downarrow}^\dagger) |0\rangle, \quad (10)$$

with  $v_\mp = J_H / \sqrt{J_H^2 + (\Delta \pm \sqrt{\Delta^2 + J_H^2})^2}$  and excitation energies  $\epsilon({}^2T_{1/2}^\Delta) = U + J_H \mp \sqrt{\Delta^2 + J_H^2}$ .

The resulting charge-excitation spectrum is shown schematically in Fig. 1(c). Although the single-occupied  $t_{2g}^1$  site of a virtual  $t_{2g}^1 t_{2g}^3$  intermediate state gives no contribution to the on-site electron-electron interaction, it can lead to an additional crystal-field energy  $\Delta$  if the electron is in the  $a$  or  $b$  orbital.

Let us first focus on the purely magnetic parts  $B_{s_i, s_j}(\hat{S}_i, \hat{S}_j)$  of the superexchange Hamiltonian, which can be determined entirely by group theoretical methods. To be precise, we consider a two-ion system in the state  $|S_A, M_A\rangle \otimes |S_B, M_B\rangle$  which can be classified by the total spin  $S_t$  and the  $z$  component  $M_t$ . Applying a hopping operator of the form  $\mathcal{H}_t = -t \sum_\sigma (c_{A\sigma}^\dagger c_{B\sigma} + \text{H.c.})$ , which preserves the quantum numbers  $S_t$  and  $M_t$  because of the spin-rotation invariance, we obtain an intermediate state  $|s_A, m_A\rangle \otimes |s_B, m_B\rangle$ , with  $s_A = S_A \pm 1/2$  and  $s_B = S_B \pm 1/2$ . The effective superexchange involving intermediate spins  $s_A$  and  $s_B$  is given by the second-order process,

$$E(S_t, s_A, s_B) = - \sum_{m_A, m_B} \frac{|\langle s_A m_A, s_B m_B | \mathcal{H}_t | S_t M_t \rangle|^2}{\Delta E}.$$

Using Clebsch-Gordan coefficients  $C_{m_1 m_2 m}^{j_1 j_2 j} = \langle j_1 j_2 m_1 m_2 | j m \rangle$ , we can express the total spin states as

$$|S_i M_i\rangle = \sum_{M_A, M_B} C_{m_A m_B M_i}^{S_A S_B S_i} |S_A, M_A\rangle \otimes |S_B, M_B\rangle.$$

Since the operators  $c_\sigma^\dagger$  and  $c_\sigma$  are irreducible tensor operators of rank 1/2 we can use the Wigner-Eckart theorem to obtain

$$\langle S_A m_A | c_{A\sigma}^\dagger | S_A M_A \rangle = \|c_A^\dagger\| C_{M_A m_A}^{S_A 1/2 S_A},$$

$$\langle S_B m_B | c_{B\sigma} | S_B M_B \rangle = \|c_B\| C_{M_B (-\sigma) m_B}^{S_B 1/2 S_B} (-1)^{1/2-\sigma},$$

where we have used  $\|\cdot\|$  as a short-hand notation for the reduced matrix elements. Using these expressions we can rewrite the exchange energy as  $E(S_i, s_A, s_B) = \frac{t^2}{\Delta E} (\|c_A^\dagger\| \cdot \|c_B\|)^2 B(S_i, s_A, s_B)$ , where we can express the function  $B$  in terms of a Wigner 6j symbol as

$$B(S_i, s_A, s_B) = - (2s_A + 1)(2s_B + 1) \left\{ \begin{matrix} S_A & s_A & \frac{1}{2} \\ s_B & S_B & S_i \end{matrix} \right\}^2,$$

which by using the relation  $S_i(S_i+1) = S_A(S_A+1) + S_B(S_B+1) + 2\hat{S}_A \hat{S}_B$  can be simplified further to

$$B_{s_A s_B} = - \frac{2}{(2s_A + 1)(2s_B + 1)} \times \left\{ \left( s_A + \frac{1}{2} \right) \left( s_B + \frac{1}{2} \right) - \text{sgn}[(s_A - s_A)(s_B - S_B)] \hat{S}_A \hat{S}_B \right\}.$$

We can evaluate this expression for  $S_A = S_B = S = 1$  for the high-spin  $s = 3/2$  and low-spin  $s = 1/2$  intermediate states to obtain the (normalized) spin-projection operators

$$B_{3/2, 1/2}(\hat{S}_i, \hat{S}_j) = -\frac{1}{3}(\hat{S}_i \hat{S}_j + 2), \quad (11)$$

$$B_{1/2, 1/2}(\hat{S}_i, \hat{S}_j) = \frac{1}{3}(\hat{S}_i \hat{S}_j - 1), \quad (12)$$

in agreement with Refs. 28 and 29. Hence, the Kugel-Komskii superexchange Hamiltonian for a given bond  $(i, j)$  can be written as

$$\mathcal{H}_{\text{KK}}^{(i,j)} = -\frac{1}{3}(\hat{S}_i \hat{S}_j + 2) \mathcal{Q}^{(1)}(\hat{T}_i, \hat{T}_j) + \frac{1}{3}(\hat{S}_i \hat{S}_j - 1) \mathcal{Q}^{(2)}(\hat{T}_i, \hat{T}_j), \quad (13)$$

where  $\mathcal{Q}^{(n)}$  are functions of orbital pseudospin operators. Their functional form can be obtained by tracking the orbital occupancies in the initial and final states during a virtual hopping process. In terms of spinless Fermi operators,  $a_i^+$  and  $b_i^+$ , increasing the occupancy of the  $a$  or  $b$  orbital on site  $i$  the pseudospin-1/2 operators acting on the ground-state manifold can be expressed as  $\hat{T}_i^z = (\hat{n}_{ia} - \hat{n}_{ib})/2$ ,  $\hat{T}_i^+ = b_i^+ a_i$ , and  $\hat{T}_i^- = a_i^+ b_i$ , where  $\hat{n}_{ia} = a_i^+ a_i$  and  $\hat{n}_{ib} = b_i^+ b_i$  with the constraint  $\hat{n}_{ia} + \hat{n}_{ib} = 1$ . Whereas it is straightforward to see that the general functional form is given by

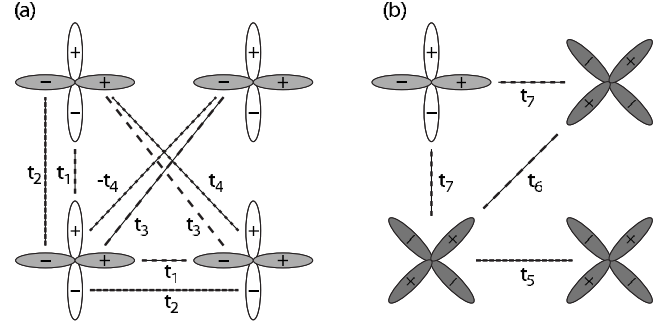


FIG. 2. Illustration of the effective hopping parameters  $t_{\alpha\beta}$ , between (a) the  $d_{xz}$  and  $d_{yz}$  orbitals and (b) those involving the  $d_{xy}$  orbitals. The projections of the  $d_{xz}$  and  $d_{yz}$  orbitals on the Fe plane are depicted in white and light gray, respectively, and the  $d_{xy}$  orbitals are shown in dark gray.

$$\begin{aligned} \mathcal{Q}^{(n)}(\hat{T}_i, \hat{T}_j) &= f_{zz}^{(n)} \hat{T}_i^z \hat{T}_j^z + \frac{1}{2} f_{+-}^{(n)} (\hat{T}_i^+ \hat{T}_j^- + \hat{T}_i^- \hat{T}_j^+) \\ &+ \frac{1}{2} f_{++}^{(n)} (\hat{T}_i^+ \hat{T}_j^+ + \hat{T}_i^- \hat{T}_j^-) + f_{zx}^{(n)} (\hat{T}_i^z \hat{T}_j^x + \hat{T}_i^x \hat{T}_j^z) + f_z^{(n)} \\ &\times (\hat{T}_i^z + \hat{T}_j^z) + f_x^{(n)} (\hat{T}_i^x + \hat{T}_j^x) + f_0^{(n)}, \end{aligned} \quad (14)$$

it is quite tedious to determine the coefficients by acting with the hopping operator  $\mathcal{H}_i$  (2) on all states in the ground-state sector and calculating the overlap of the resulting states projected on the different intermediate states listed above. The resulting explicit expressions are given in Appendix A.

### C. Hopping and resulting Hamiltonian

In Sec. II B we have derived the general KK superexchange Hamiltonian only assuming the effective hopping matrices to be symmetric,  $t_{\alpha\beta} = t_{\beta\alpha}$ . In order to write down the spin-orbital model specific to the pnictide planes we have to use the corresponding hopping parameters. We use the Slater-Koster integrals<sup>32</sup> along with the geometry of the Fe-As planes to determine all the hopping parameters involving the three  $t_{2g}$  orbitals on the nearest-neighbor and next-nearest-neighbor Fe sites. This considerably reduces the number of independent hopping parameters that enter the Hamiltonian. The direct  $d$ - $d$  hoppings are considered to be much smaller therefore we use hoppings via the As  $p$  orbitals only which are given in Appendix B and depend on the direction cosines  $l, m, n$  of the As-Fe bond, as well as on the ratio  $\gamma = (pd\pi)/(pd\sigma)$ .<sup>14(d),33,34</sup> These resulting effective hopping matrix elements between the  $t_{2g}$  Fe orbitals are shown schematically in Fig. 2 and can be parametrized by the lattice parameter  $\lambda = |n/l|$  and  $\gamma$ .

In Fig. 3 the dependence of the hopping matrix elements on the ratio  $\gamma = (pd\pi)/(pd\sigma)$  is shown for a lattice parameter  $\lambda = 0.7$  which is slightly below the value resulting from the Fe-Fe spacing and the distance of the As ions to the Fe planes. Over a realistic range  $-0.2 \leq \gamma \leq 0.2$  we find a very strong dependence of the hopping amplitudes on  $\gamma$  and therefore expect the stability of possible phases to depend crucially on  $\gamma$ . This parameter cannot be obtained by geometri-

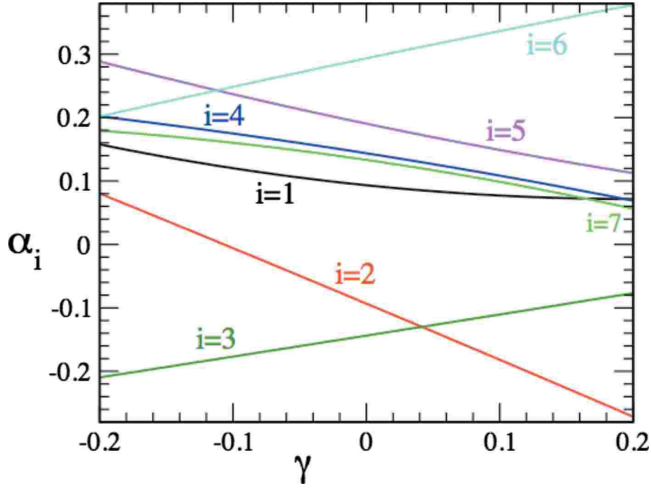


FIG. 3. (Color online) Various hopping parameters  $\alpha_i := t_i/t$  as illustrated in Fig. 2 as a function of the ratio  $\gamma = (pd\pi)/(pd\sigma)$  for the lattice parameter  $\lambda = 0.7$ .

cal considerations but depends for instance on how strongly the orbitals delocalize.

Having specified the effective hopping parameters  $\alpha_i := t_i/t$  between the Fe orbitals for nearest and next-nearest neighbors (see Fig. 2) which are parametrized entirely by the ratio  $\gamma = (pd\pi)/(pd\sigma)$  and the lattice parameter  $\lambda = |n/l|$ , we can now write down the effective KK model for the Fe planes. For convenience, we rewrite the Hamiltonian in the form

$$\mathcal{H}_{\text{KK}} = J \sum_{(i,j)} \left[ \frac{1}{2} (\hat{S}_i \hat{S}_j + 1) \hat{\Omega}_{(i,j)} + \hat{\Gamma}_{(i,j)} \right], \quad (15)$$

introducing an overall energy scale  $J = 4t^2/U$ . The orbital bond operators are defined as  $\hat{\Omega} = \frac{U}{6r^2} (Q^{(2)} - Q^{(1)})$  and  $\hat{\Gamma} = -\frac{U}{12r^2} (Q^{(1)} + 2Q^{(2)})$  and depend on the effective couplings  $\alpha_i$ , the relative strength of Hund's coupling  $\eta = J_H/U$ , and the crystal-field splitting  $\delta = \Delta/U$ . For the nearest-neighbor bonds along  $\hat{x}$  and  $\hat{y}$  along the  $\hat{x} \pm \hat{y}$  diagonals the operators are given in Appendix C.

### III. CLASSICAL PHASE DIAGRAMS

In this section we discuss the phase diagrams of the spin-orbital Hamiltonian in the classical limit. We have four parameters that enter the model:  $\lambda$  and  $\gamma$  determine the relative strength of various hopping parameters and  $\eta$  and  $\delta$  enter via the energy denominators. Zero-temperature phase transitions are discussed in Sec. II A, Sec. II B is devoted to the understanding of finite temperature transitions, and Sec. II C analyzes the phases in terms of the corresponding spin-only and orbital-only models.

The results that we discuss below demonstrate that the Hamiltonian is highly frustrated in the spin and orbital variables. While the spin frustration is largely due to the competing interactions between nearest and next-nearest neighbors, the frustration in orbital sector is more intrinsic and exists within a single bond in the Hamiltonian. The spin

$(\pi, 0)$  state is found to be stable over a wide range of parameter space due to the strong nnn AF coupling. However, depending on the parameters, there are three possible orderings of the orbitals that accompany the spin-stripe order. Two out of these three orbital ordering patterns break the in-plane symmetry of the lattice and hence are likely candidates for explaining the orthorhombic transition observed in the parent compounds.

#### A. Zero temperature

Since the effective KK Hamiltonian derived in Sec. II contains a large number of competing terms it is almost impossible to anticipate what kind of spin-orbital orderings are realized for different parameter values, in particular since the signs and relative strengths of the effective hoppings  $\alpha_i$  between nearest-neighbor and next-nearest-neighbor Fe orbitals crucially depend on the ratio  $\gamma = (pd\pi)/(pd\sigma)$  as pictured in Fig. 3. While the parameters  $\alpha_1$ ,  $\alpha_4$ , and  $\alpha_7$  do not show large relative changes over the range of  $\gamma$  shown in the figure, there are very clear crossings between  $\alpha_2$  and  $\alpha_3$  and  $\alpha_5$  and  $\alpha_6$ .

Recall that  $\alpha_5$  and  $\alpha_6$  are the hoppings between nearest and next-nearest neighbors involving orbital  $|c\rangle := |xy\rangle$ . If we infer the spin order arising purely from the nondegenerate  $|c\rangle$  orbital, it suggests that the spin state should be  $(\pi, 0)$ -ordered for  $\alpha_5^2 < 2\alpha_6^2$  and  $(\pi, \pi)$ -ordered otherwise. Therefore, this would imply that as  $\gamma \rightarrow -0.2$  the magnetic superexchange resulting from the  $|c\rangle$  orbitals only favors  $(\pi, \pi)$  antiferromagnetism, whereas the  $(\pi, 0)$  stripe AF becomes favorable for  $\gamma \rightarrow 0.2$ .

A similar spin-only analysis for the degenerate orbitals  $|a\rangle, |b\rangle$  is not possible, and one has to treat the full spin-orbital Hamiltonian in order to find the ground states. Nevertheless, the complicated variations in the hopping parameters already suggest that we can expect a very rich and complex phase diagram for the ground state of the spin-orbital Hamiltonian. In particular in the region of intermediate  $\gamma$  where the magnetic superexchange model resulting from the  $|c\rangle$  orbitals only becomes highly frustrated, we expect the magnetic ordering to depend crucially on the orbital degrees of freedom.

We first look at the classical ground states of this model. We make use of classical Monte Carlo method in order to anneal the spin and orbital variables simultaneously, starting with a completely random high-temperature configuration. Using this method we identify the various ground states that exist for a combination of model parameters. In order to obtain a ground-state phase diagram, we minimize the total energy for a set of variational states which also include all the Monte Carlo ground states obtained for different choice of parameters.

Figure 4 shows the resulting  $T=0$  phase diagram for varying  $\eta = J_H/U$  and  $\gamma = (pd\pi)/(pd\sigma)$ . The lattice parameter  $\lambda$  is fixed to 0.7, which is close to the experimental value for the oxypnictides. The crystal-field splitting between the  $|c\rangle$  and the  $|a\rangle, |b\rangle$  orbitals is considered to be very small,  $\delta = \Delta/U = 0.01$ . As expected, a large number of phases are present in the phase diagram.

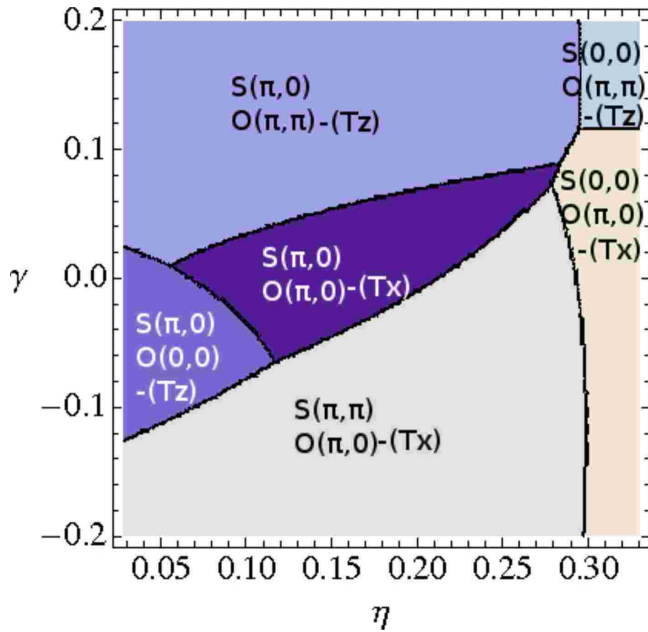


FIG. 4. (Color online)  $\eta$ - $\gamma$  phase diagram for  $\lambda=0.7$  and  $\delta=0.01$ .  $\eta=J_H/U$  and  $\gamma=(pd\pi)/(pd\sigma)$ . The phases are denoted by their ordering wave vectors in the spin and orbital variables.  $T_z$  or  $T_x$  refers to the component of the orbital pseudospin that is saturated in the ordered state.

With increasing  $\gamma$  we indeed find a transition from a  $(\pi, \pi)$  to a  $(\pi, 0)$  antiferromagnet as suggested from the analysis of the frustrated magnetic superexchange model involving only the  $|c\rangle$  orbitals. This is not surprising since the corresponding couplings  $\alpha_5^2$  and/or  $\alpha_6^2$  are sufficiently strong and as  $\gamma \rightarrow 0.2$  the biggest hopping element is in fact given by  $\alpha_6$  between next-nearest-neighbor  $|c\rangle$  orbitals (see Fig. 3). Whereas the  $(\pi, 0)$  stripe magnet for large  $\gamma$  is accompanied by an antiferro-orbital ordering of the  $T_z$  components corresponding to a checkerboard arrangement of the  $|a\rangle$  and  $|b\rangle$  orbitals [see Fig. 5(c)] for intermediate small  $\gamma$ , we find two  $(\pi, 0)$  magnetic phases possessing orbital orderings which are likely to break the in-plane symmetry of the lattice structure.

For small  $\eta$  we find a ferro-orbital arrangement of the  $T_z$  components corresponding to the formation of chains along the ferromagnetically coupled spin directions [see Fig. 5(a)]. The existence of this orbital order crucially depends on the pre-existence of a spin-stripe state, which generates magnetic-field-like terms for the orbital pseudospins. This will be discussed in detail when we try to understand the thermal phase transitions. For larger  $\eta$  the orbital order changes to an orbital- $(\pi, 0)$  tweed pattern with a condensation of the  $T_x$  components. This corresponds to the formation of orbital zigzag chains along the antiferromagnetically coupled spin direction as pictured in Fig. 5(b). Interestingly, the stripes in the magnetic and orbital sectors have the same orientation, contrary to the conventional Goodenough-Kanamori rules. However, since we are dealing with a highly frustrated spin-orbital model involving nearest-neighbor and next-nearest-neighbor bonds, these naive rules are not expected to hold. The tweed orbital order is expected to lead to

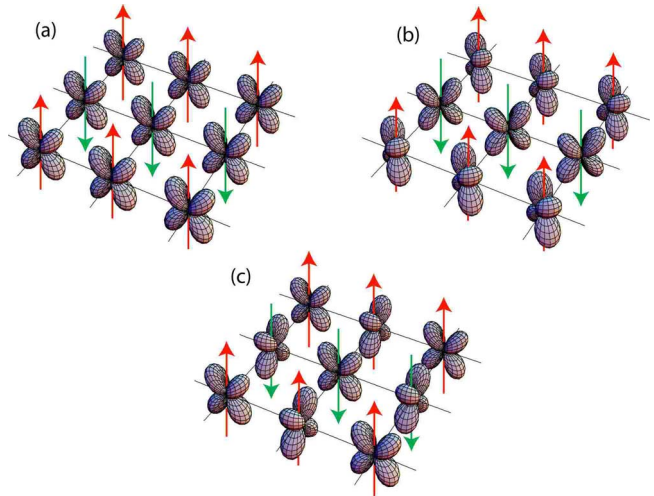


FIG. 5. (Color online) Schematic pictures of the three ground-state orbital ordering patterns that accompany the spin-stripe phase. (a) Orbital ferro, (b) orbital stripe, and (c) orbital antiferro.

a displacement pattern of the As ions, which can in principle be observed in x-ray diffraction experiments. The tweed orbital pattern should show up as a higher-order structural Bragg peak at  $(\pi, 0)$ . The orbital order might also be directly visible resonant x-ray diffraction at the iron  $K$ -edge, a technique that was pioneered in the manganites,<sup>35–37</sup> and is nowadays available for all transition-metal  $K$ -edges, in particular the iron one.<sup>38</sup> Polarization analysis and azimuthal angle dependence can distinguish between charge, spin, and orbital contributions to the resonant signal<sup>35</sup> which gives the possibility in the iron pnictides to single out the tweed orbital pattern.

The orbital-stripe order persists to the regime of larger negative  $\gamma$  where the magnetic order changes to the  $(\pi, \pi)$  antiferromagnet. This shows that the orbital tweed state does not have spin- $(\pi, 0)$  order as a prerequisite, and therefore this orbital order can, in principle, exist at temperatures higher than the spin transition temperatures. In the regime of large Hund's coupling,  $\eta \geq 0.3$  the system becomes ferromagnetic. This tendency is easy to understand since in the limit  $\eta \rightarrow 1/3$  the charge-transfer gap closes and the KK model is dominated by processes involving the low-lying  $^4A_2$  high-spin multiplet favoring a ferromagnetic superexchange.

Let us further explore how the ground-state phase diagram changes as we vary the lattice parameter  $\lambda$  and the crystal-field splitting  $\delta$ . Figure 6 shows the same phase diagram as in Fig. 4 but for a slightly larger separation of the As ions to the Fe-planes,  $\lambda=0.8$ . The two interesting phases with magnetic  $(\pi, 0)$  and orbital-stripe and orbital ferro-orderings do not appear in this phase diagram indicating that the stability of these phases crucially depends on the relative strength of nearest and next-nearest hoppings which can be tuned by  $\lambda$ . Presence of a tetracritical point is an interesting feature in this phase diagram.

Finally, we analyze the dependence on the crystal-field splitting  $\delta=\Delta/U$  which so far we assumed to be tiny. We do not find any qualitative change in the ground-state phase diagram with increasing  $\delta$ . In particular, there are no new phases that appear and therefore the crystal-field splitting

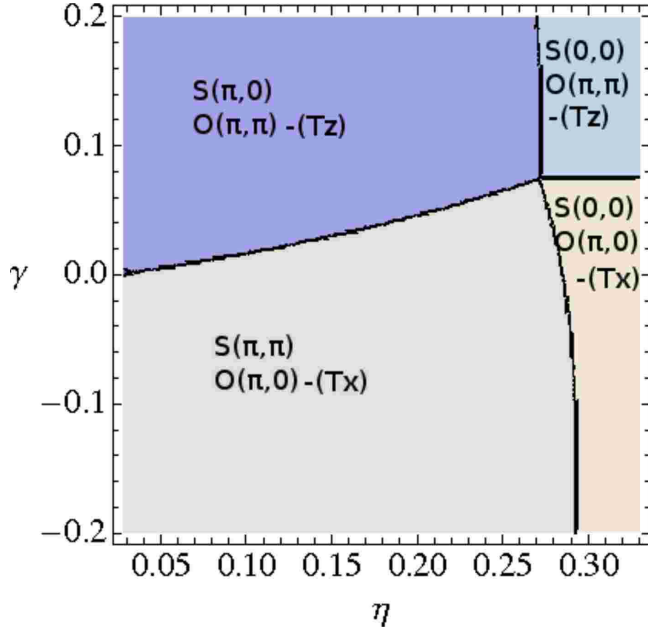


FIG. 6. (Color online)  $\eta$ - $\gamma$  phase diagram for  $\lambda=0.8$  and  $\delta=0.01$ . Note that the orbital-ordered states that break the orthorhombic symmetry do not exist for this choice of  $\lambda$ .

does not seem to be a crucial parameter. For example, the phase diagram in the  $\eta$ - $\delta/\eta$ -plane for  $\lambda=0.7$  and  $\gamma=-0.05$  shown in Fig. 7 indicates that a change in  $\delta$  only leads to a small shift of the phase boundaries.

### B. Finite temperature

To obtain the transition temperatures for the various phase transitions, we track different order parameters as a function

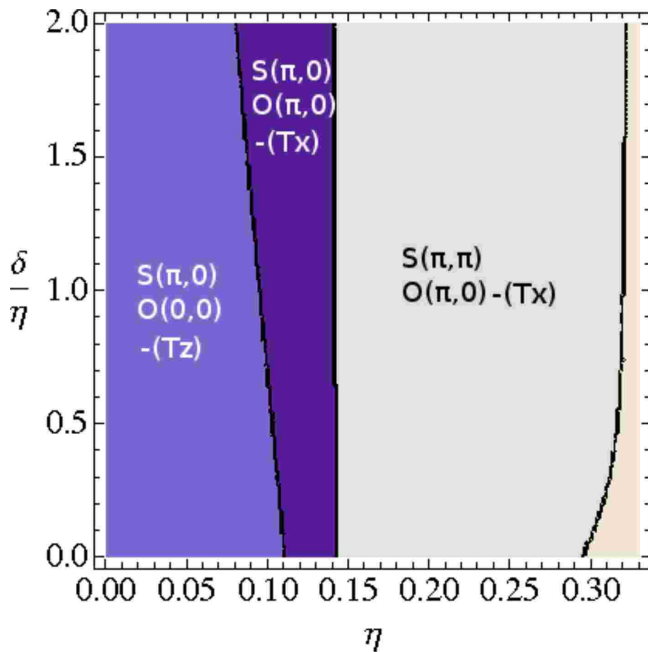


FIG. 7. (Color online)  $\eta$ - $\delta/\eta$  phase diagram for  $\lambda=0.7$  and  $\gamma=(pd\pi)/(pd\sigma)=-0.05$ . This phase diagram illustrates the point that  $\delta$  is not a crucial parameter in the Hamiltonian.

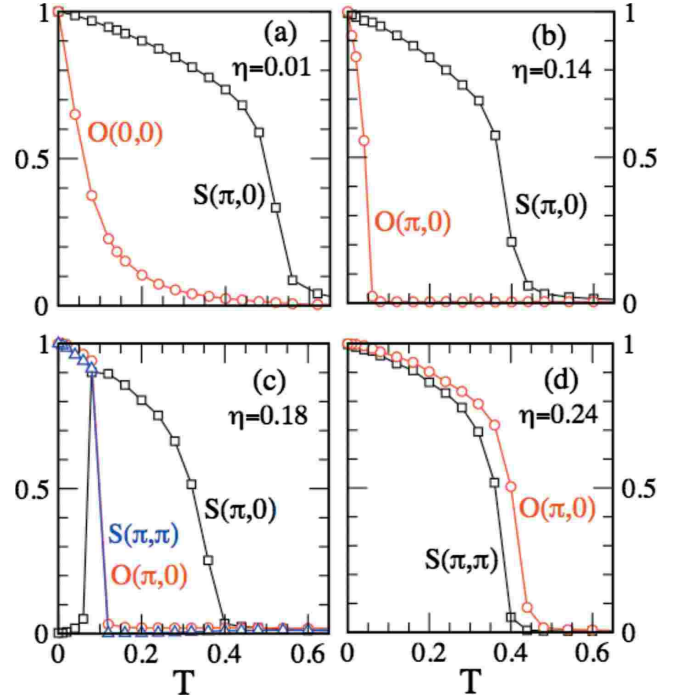


FIG. 8. (Color online) Relevant structure factors as a function of temperature for different values of  $\eta$ . The lattice parameter and the relative strength of  $\sigma$  and  $\pi$  hopping are fixed as  $\lambda=0.7$  and  $\gamma=-0.05$ , respectively.

of temperature during Monte Carlo annealing where we measure the temperature in units of the energy scale  $J$ . For example, the spin structure factor is defined as

$$S(\mathbf{q}) = \frac{1}{N^2} \sum_{i,j} \langle \mathbf{S}_i \cdot \mathbf{S}_j \rangle_{\text{av}} e^{i\mathbf{q} \cdot (\mathbf{r}_i - \mathbf{r}_j)}, \quad (16)$$

where  $\langle \dots \rangle_{\text{av}}$  denotes thermal averaging and  $N$  is the total number of lattice sites. The orbital structure factor  $O(\mathbf{q})$  is defined analogously by replacing the spin variables by the orbital variables in the above expression. Depending on the ground state, different components of these structure factors show a characteristic rise upon reducing temperature.

We fix  $\delta=0.01$ ,  $\lambda=0.7$ , and  $\gamma=-0.05$  and track the temperature dependence of the system for varying  $\eta$ . For  $T=0$  this choice of parameters corresponds to a cut of the phase diagram shown in Fig. 4 through four different phases including the two  $(\pi,0)$  stripe AFs with orbital orderings breaking the in-plane lattice symmetry.

In Fig. 8 the temperature dependence of the corresponding structure factors is shown for representative values of Hund's rule coupling  $\eta$ . For small values of  $\eta$  the ground state corresponds to the orbital-ferro and spin-stripe states as shown in the phase diagram in Fig. 4. Figure 8(a) shows the temperature dependence of  $S(\pi,0)$  and  $O(0,0)$  which are the order parameters for the spin-stripe and orbital-ferro states, respectively. While the  $S(\pi,0)$  leads to a characteristic curve with the steepest rise at  $T \sim 0.5$ , the rise in  $O(0,0)$  is qualitatively different. In fact there is no transition at any finite  $T$  in the orbital sector. We can still mark a temperature below which a significant orbital-ferro ordering is present. The ori-

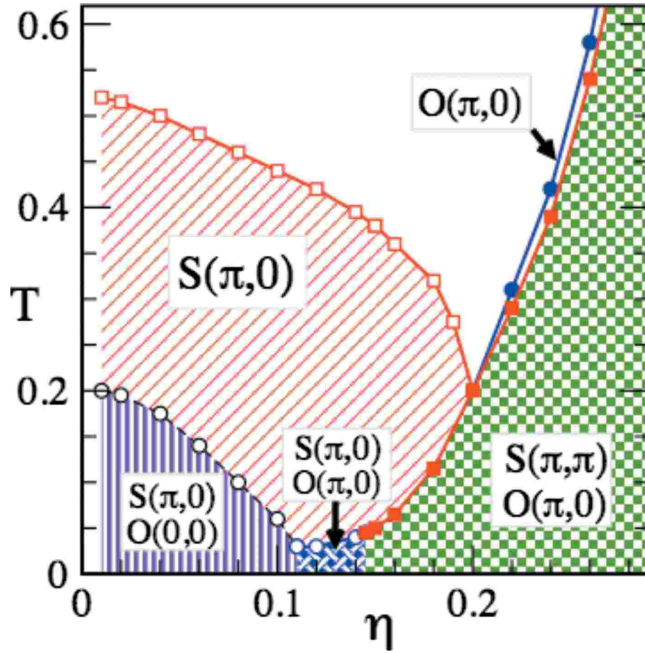


FIG. 9. (Color online)  $T$ - $\eta$  phase diagram for  $\delta=0.01$ ,  $\lambda=0.7$ , and  $\gamma=-0.05$ .

gin of this behavior lies in the presence of a Zeeman-type term for the orbital pseudospin.

For  $\eta=0.15$ , the phase diagram of Fig. 4 suggests a state with stripe ordering in both spin and orbital variables. We show the temperature dependence of  $S(\pi,0)$  and  $O(\pi,0)$  in Fig. 8(b). In this case both the spin and orbital variables show a spontaneous ordering, with the spins ordering at a much higher temperature. An interesting sequence of transitions is observed upon reducing temperature for  $\eta=0.18$  [see Fig. 8(c)]. This point lies close to the phase boundary between spin-stripe and spin-ferro states with the orbital-stripe ordering. The spin-stripe order parameter  $S(\pi,0)$  shows a strong rise near  $T=0.4$ . The orbital-stripe order sets in at  $T \sim 0.15$ . The onset of this orbital order kills the spin-stripe order. Instead, we find that the  $(\pi, \pi)$  components of the spin structure factor shows a strong rise along with the  $(\pi,0)$  component of the orbital structure factor. Finally for  $\eta=0.24$  the orbital-stripe ordering is accompanied by the spin antiferro-ordering, with the orbital ordering setting in at slightly higher temperatures [see Fig. 8(d)].

The results shown in Fig. 8 are summarized in the  $T$ - $\eta$  phase diagram shown in Fig. 9. For small  $\eta$ , the ground state is spin-stripe and orbital-ferro ordered. While the spin order occurs at higher temperatures, there is no genuine transition to the orbital-ferro state. The orbital-ferro state is driven by the presence of a magnetic-field-like term for the orbital pseudospin in the Kugel-Khomskii Hamiltonian. The stability of the orbital-ferro state crucially depends on the presence of the spin-stripe order. The dotted line joining the black circles in the small- $\eta$  range is only to indicate the temperature below which the orbital-ferro order is significant. This typical temperature scale reduces with increasing  $\eta$  until the system finds a different ground state for the orbital variables. Note that the temperature scales involved are very small ow-

ing to the highly frustrated nature of the orbital model, nevertheless there is no zero-temperature transition in this purely classical limit.

The spin-stripe state remains stable with the transition temperature reducing slightly. The transition temperature for the orbital-stripe state increases upon further increasing  $\eta$ . For  $0.15 < \eta < 0.2$ , multiple thermal transitions are found for the magnetic state. The spin-stripe order which sets in nicely at  $T \sim 0.35$  is spoiled by the onset of orbital-stripe state, which instead stabilizes the spin  $(\pi, \pi)$  state. Beyond  $\eta = 0.2$ , The orbital-stripe state occurs together with the spin antiferrostate, with the spin-ordering temperatures slightly lower than those for the orbital ordering. For  $\eta > 0.3$ , the spin state becomes ferromagnetic.

### C. Corresponding orbital-only and spin-only models

In an attempt to provide a clear understanding of the spin-ordered and orbital-ordered phases, we derive the orbital (spin) model that emerges by freezing the spin (orbital) states. For fixed spin correlations, the orbital model can be written as

$$\begin{aligned} \mathcal{H}_O = & \sum_{\mu} K_x^{\mu\mu} \sum_{\langle i,j \rangle_x} T_i^{\mu} T_j^{\mu} + \sum_{\mu} K_y^{\mu\mu} \sum_{\langle i,j \rangle_y} T_i^{\mu} T_j^{\mu} \\ & + \sum_{\mu} K_d^{\mu\mu} \sum_{\langle\langle i,j \rangle\rangle} T_i^{\mu} T_j^{\mu} + K^z \sum_i T_i^z. \end{aligned} \quad (17)$$

Here and below  $\langle \cdot, \cdot \rangle$  and  $\langle\langle \cdot, \cdot \rangle\rangle$  denote bonds between nearest-neighbor and next-nearest-neighbor pseudospins on the square lattice, respectively.  $\mu$  denotes the component of the orbital pseudospin. The effective exchange couplings for this orbital-only model are shown in Fig. 10 as a function of Hund's coupling  $\eta = J_H/U$  with the other parameters fixed as  $\delta=0.01$ ,  $\gamma=-0.05$ , and  $\lambda=0.7$ , as before. The solid lines are obtained by fixing the spin degrees of freedom by the classical ground-state configurations of the corresponding phases. For comparison, the effective couplings for disordered spins are shown by dashed lines.

Similarly, we can freeze the orbital degrees of freedom to obtain an effective Heisenberg model for spins,

$$\mathcal{H}_S = J_x \sum_{\langle i,j \rangle_x} \mathbf{S}_i \cdot \mathbf{S}_j + J_y \sum_{\langle i,j \rangle_y} \mathbf{S}_i \cdot \mathbf{S}_j + J_d \sum_{\langle\langle i,j \rangle\rangle} \mathbf{S}_i \cdot \mathbf{S}_j. \quad (18)$$

The coupling constants  $J_x$ ,  $J_y$ , and  $J_d$  for spins are plotted in Fig. 11.

Let us try to understand the phase diagram of Fig. 9 in terms of these coupling constants. We begin with the small- $\eta$  regime where the ground state is spin stripe and orbital ferro. Approaching from the high-temperature limit, we should look at the spin (orbital) couplings with disordered orbitals (spins). The strongest constants turn out to be  $J_d$ , which is slightly larger than  $J_x$  and  $J_y$ , all three being antiferromagnetic. This suggests that the system should undergo a transition to a spin-stripe state consistent with the phase diagram. The coupling constants of the orbital model are much weaker in the small- $\eta$  regime. The largest constant is  $K_d^{xx}$  suggesting an orbital-stripe order. However, since the spin-stripe state sets in at higher temperatures, in order to determine the or-

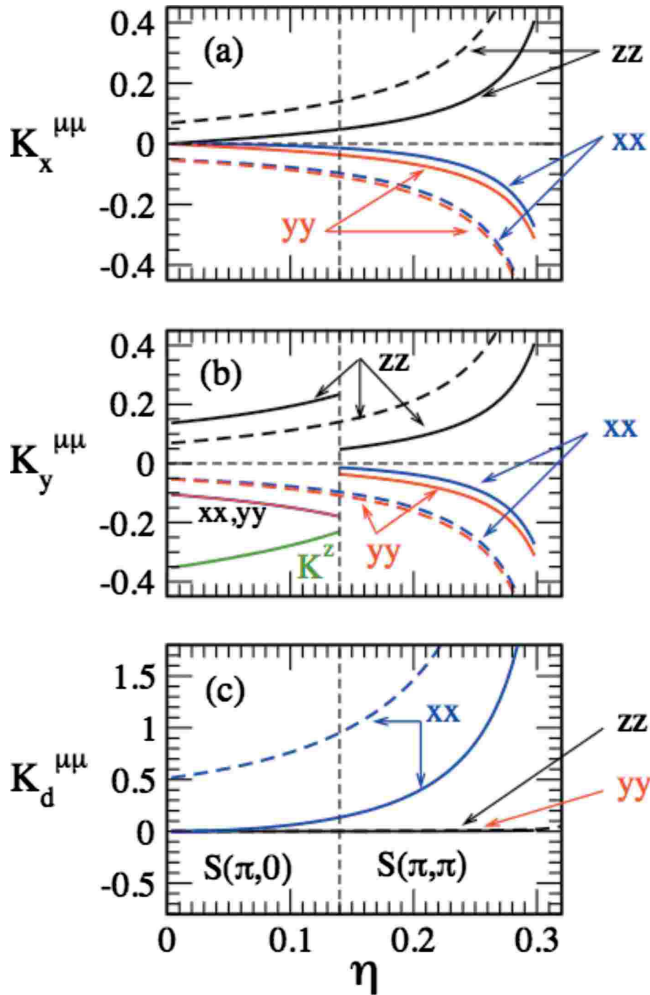


FIG. 10. (Color online) The coupling constants as a function of  $\eta=J_H/U$  for the orbital-only model with frozen spin correlations for  $\delta=0.01$ ,  $\gamma=-0.05$ , and  $\lambda=0.7$ . The couplings along  $x$ ,  $y$ , and diagonal directions are plotted in panels (a), (b), and (c), respectively. The single site term is plotted in (b) to indicate that this term arises due to a ferromagnetic bond along  $y$  direction. The solid lines correspond to the ground-state spin order and the dashed lines are for a paramagnetic spin state. The vertical dashed line indicates the location in  $\eta$  of the phase transition from spin-stripe to spin-antiferro state as seen in Fig. 9.

orbital order one should look at the coupling constants corresponding to the spin-stripe state. There are three main effects (compare the solid and dashed lines in the low  $\eta$  regime in Fig. 10), (i)  $x$  and  $y$  directions become inequivalent in the sense that the couplings along  $x$  are suppressed while those along  $y$  are enhanced, (ii) the diagonal couplings are reduced strongly, and (iii) a single-site term is generated which acts as magnetic field for the orbital pseudospins. It is in fact this single-site term that controls the ordering of the orbitals at low temperatures. This also explains the qualitatively different behavior of the orbital-ferro-order parameter observed in Fig. 8(a). Within the spin-stripe order, the single-site term becomes weaker with increasing  $\eta$  whereas the diagonal term increases. This leads to a transition in the orbital sector from an orbital-ferro to an orbital-stripe phase near  $\eta=0.11$ . The region between 0.14 and 0.2 in  $\eta$  is very interesting.

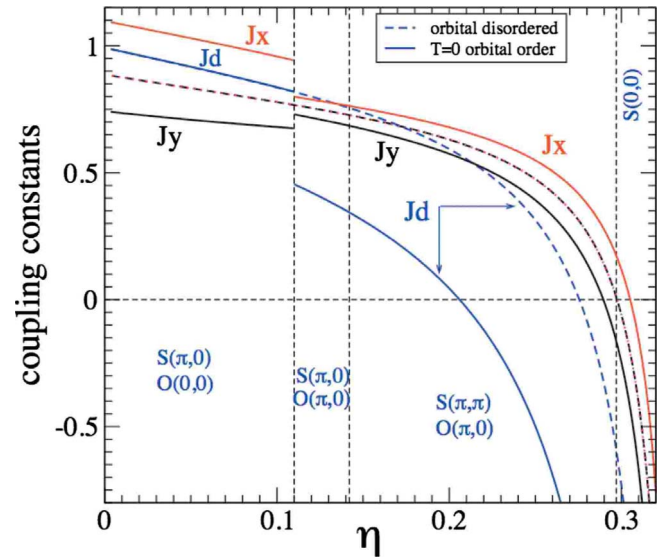


FIG. 11. (Color online) Effective exchange couplings  $J_x$  and  $J_y$  for nearest-neighbor and  $J_d$  for next-nearest-neighbor spins as a function of  $\eta=J_H/U$  for  $\delta=0.01$ ,  $\gamma=-0.05$ , and  $\lambda=0.7$ . The solid lines correspond to the couplings resulting for the corresponding orbital ground states, whereas the dashed lines correspond to the orbitally disordered case. Note that for the orbitally disordered case  $J_x=J_y$  for all values of  $\eta$ . The vertical dashed line indicates the location in  $\eta$  of the various phase transition as seen in Fig. 9.

Approaching from the high temperature the spins order into the stripe state but as soon as the orbitals order into stripe state at lower temperature the diagonal couplings  $J_d$  are strongly reduced and become smaller than  $J_y/2$ . This destabilizes the spin-stripe state and leads to a spin antiferro-ordering. For larger  $\eta$  the orbital ordering occurs at higher temperature. There is another transition slightly below  $\eta=0.3$  where spins order into a ferro state. This is simply understood as  $J_x=-J_y$  from the coupling constants of the Heisenberg model.

#### IV. MAGNETIC EXCITATION SPECTRA

We now set out to compute the magnetic excitation spectra, treating the orbital pseudospins as classical and static variables. Fixing the orbital degrees of freedom for a given set of parameters by the corresponding ground-state configuration, we are left with an  $S=1$  Heisenberg model written in Eq. (18). The exchange couplings are plotted in Fig. 11. Assuming the presence of local moments, such  $J_1$ - $J_2$  models have been motivated and used to rationalize the  $(\pi,0)$  magnetism in the iron pnictides<sup>39</sup> and been used subsequently to calculate the magnetic excitation spectra,<sup>40,41</sup> where the incorporation of a relatively strong anisotropy between the nearest-neighbor couplings turned out to be necessary to understand the low-energy spin-wave excitations.<sup>41</sup>

In the presence of orbital ordering such an anisotropy of the effective magnetic exchange couplings appears naturally. Both, the orbital-ferro and the orbital-stripe orders lead to a sizable anisotropy in the nearest-neighbor couplings,  $J_x$  and

$J_y$ , where the anisotropy is much stronger for the orbital-ferro order (see Fig. 11). An even more drastic effect is the huge suppression of  $J_d$  in the orbital-stripe regime.

On a classical level, the magnetic transitions are easily understood in the spin-only model (18) as discussed before. The transition from the stripe AF to the  $(\pi, \pi)$  AF at  $\eta \approx 0.14$  occurs exactly at the point where  $J_y = 2J_d$ , whereas the transition from  $(\pi, \pi)$  to ferromagnetic order at  $\eta \approx 0.3$  corresponds to the point  $J_x = -J_y$ .

We proceed to calculate the magnetic excitation spectra in the  $\mathbf{Q}=(\pi, 0)$  and  $(\pi, \pi)$  phases within a linear spin-wave approximation. The classical ground states are given by  $\mathbf{S}_r = S(0, 0, \sigma_r)$ , with  $\sigma_r = \exp(i\mathbf{Q}\mathbf{r}) = \pm 1$ . After performing a simple spin rotation,  $S^x = \tilde{S}_r^x$ ,  $S^y = \sigma_r \tilde{S}_r^y$ , and  $S^z = \sigma_r \tilde{S}_r^z$ , we express the rotated spin operators by Holstein-Primakoff bosons,  $\tilde{S}^+ = \sqrt{2S - \hat{n}}b$ ,  $\tilde{S}^- = b^\dagger \sqrt{2S - \hat{n}}$ , and  $\tilde{S}^z = S - \hat{n}$ , with  $\hat{n} = b^\dagger b$  to obtain the spin-wave Hamiltonian,

$$\mathcal{H} = S \int_{\mathbf{q}} \{A_{\mathbf{q}}(b_{\mathbf{q}}^\dagger b_{\mathbf{q}} + b_{-\mathbf{q}} b_{-\mathbf{q}}^\dagger) + B_{\mathbf{q}}(b_{\mathbf{q}}^\dagger b_{-\mathbf{q}}^\dagger + b_{-\mathbf{q}} b_{\mathbf{q}})\},$$

with

$$A_{\mathbf{q}} = \left[ -J_x \cos Q_x + J_x \frac{1 + \cos Q_x}{2} \cos q_x - J_d \cos Q_x \cos Q_y \right. \\ \left. + \frac{J_d}{2} (1 + \cos Q_x \cos Q_y) \cos q_x \cos q_y \right] + x \leftrightarrow y,$$

$$B_{\mathbf{q}} = J_x \frac{1 - \cos Q_x}{2} \cos q_x + J_y \frac{1 - \cos Q_y}{2} \cos q_y \\ + J_d (1 - \cos Q_x \cos Q_y) \cos Q_x \cos Q_y,$$

yielding the spin-wave dispersion  $\omega_{\mathbf{q}} = S \sqrt{A_{\mathbf{q}}^2 - B_{\mathbf{q}}^2}$  and the inelastic structure factor at zero temperature,<sup>42</sup>

$$S_{\text{inel}}(\mathbf{q}, \omega) = \sqrt{\frac{1 - \gamma_{\mathbf{q}}}{1 + \gamma_{\mathbf{q}}}} \delta(\omega - \omega_{\mathbf{q}}), \quad (19)$$

with  $\gamma_{\mathbf{q}} = B_{\mathbf{q}}/A_{\mathbf{q}}$ . The resulting excitation spectra are shown in Fig. 12 for different values of  $\eta$ . In the case of disordered orbitals, the  $(\pi, 0)$  antiferromagnet order is stable up to  $\eta \approx 0.25$ . Since  $J_x = J_y$ , the spectrum is gapless not only at the ordering wave vector  $(\pi, 0)$  but also at the antiferromagnetic wave vector  $(\pi, \pi)$ . However, the spectral weight is centered close to the ordering wave vector and goes strictly to zero at the antiferromagnetic wave vector. In the presence of orbital ordering the next-nearest-neighbor couplings are anisotropic  $J_x > J_y$  which in the case of the  $(\pi, 0)$ -AF leads to a gap at the antiferromagnetic wave vector,  $\Delta_{(\pi, \pi)} = 2\sqrt{(2J_d - J_y)(J_x - J_y)}$ . Since the anisotropy and the diagonal exchange are large in the orbital-ferro state we find a very big gap at  $(\pi, \pi)$ . This gap reduces drastically for bigger  $\eta$  where the orbital-stripe state becomes favorable. Due to the large reduction in  $J_d$  and also of the anisotropy, the gap is considerably smaller and continuously goes to zero as we approach the transition to the  $(\pi, \pi)$ -AF at  $\eta \approx 0.14$  where  $2J_d - J_y = 0$ . This of course also leads to a strong anisotropy of the spin-wave velocities,  $v_y/v_x = \sqrt{(2J_d - J_y)/(2J_d + J_x)}$ . On

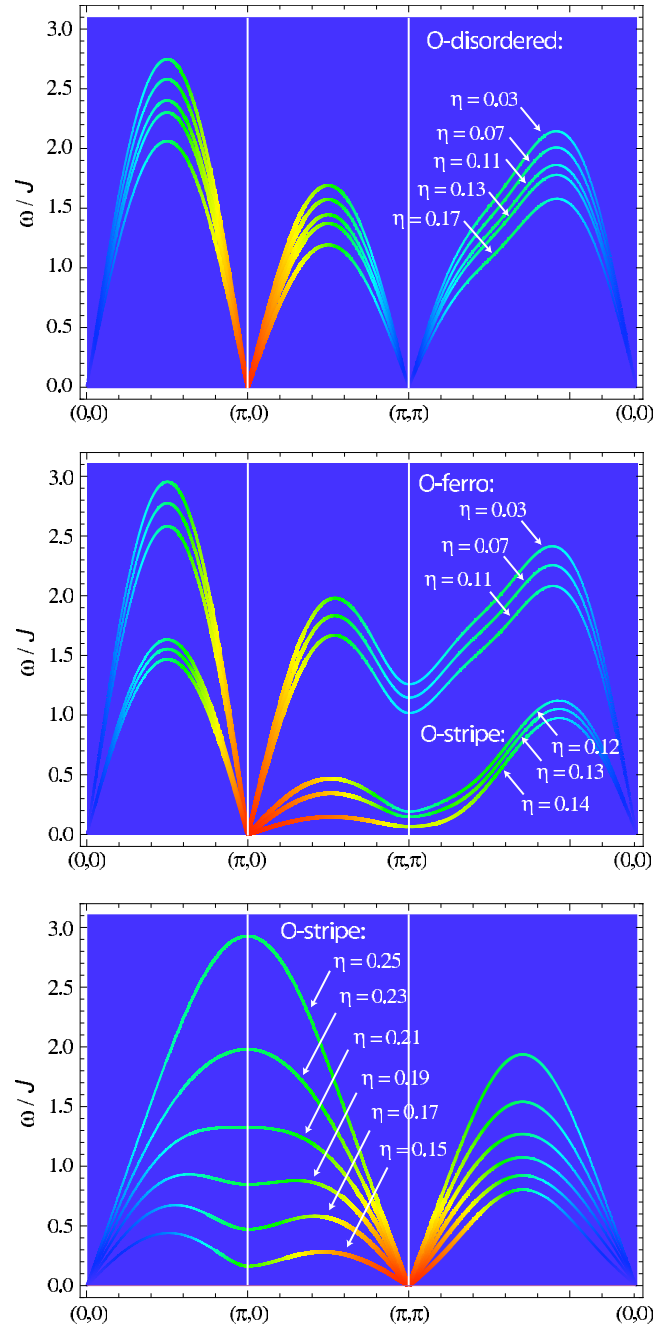


FIG. 12. (Color online) Spin-wave excitation spectra for different values of  $\eta$ . Top:  $(\pi, 0)$  magnet for disordered orbitals. The spectral weights are coded by line thickness and color; high intensity corresponds to red, low intensity to blue. Middle:  $(\pi, 0)$  magnet for orbital-ferro ( $\eta=0.03, 0.07, 0.11$ ) and orbital-stripe ( $\eta=0.12, 0.13, 0.14$ ) orders. Bottom:  $(\pi, \pi)$  magnet with orbital-stripe order ( $\eta=0.15, 0.17, \dots$ ).

approaching the magnetic transition we find a significant softening of modes along the  $(\pi, 0) - (\pi, \pi)$  direction which leads to a considerable reduction in magnetic moments close to the transition.

## V. DISCUSSION AND CONCLUSIONS

In the preceding we have derived and studied a spin-orbital Kugel-Khomskii Hamiltonian relevant to the Fe-As

planes of the parent compound of the iron superconductors. A variety of interesting spin-ordered and orbital-ordered phases exist over a physical regime in parameter space. Due to the peculiarities of the pnictide lattice and this particular crystal-field state, we show that the relevant Kugel-Khomskii model is of a particularly interesting kind.

The essence of the spin-charge-orbital physics is *dynamical frustration*. With so many “wheels in the equation” it tends to be difficult to find solutions that satisfy simultaneously the desires of the various types of degrees of freedom in the problem. This principle underlies the quite complex phase diagrams of, for instance, manganites. But this dynamical frustration is also a generic property of the spin-orbital models describing the Jahn-Teller degenerate Mott insulators. In the classic Kugel-Khomskii model<sup>43</sup> describing  $e_g$  degenerate  $S=1/2$   $3d^9$  systems of cubic 3D systems, Feiner *et al.*<sup>44,45</sup> discovered a point in parameter space where on the classical level this frustration becomes perfect. In the present context of pnictides this appears as particularly relevant since this opens up the possibility that quantum fluctuations can become quite important.

We propose two specific orbital-ordered phases that explain the orthorhombic transition observed in the experiments. These are orbital-ferro and orbital-stripe states. The orbital-stripe order is particularly interesting since it leads to a spin model that provides possible explanation for the reduction in magnetic moment. It is our main finding that in the idealized pnictide spin-orbital model the conditions appear optimal for the frustration physics to take over. We find large areas in parameter space where frustration is near perfect. The cause turns out to be a mix of intrinsic frustration associated with having  $t_{2g}$ -type orbital degeneracy and the frustration of a geometrical origin coming from the pnictide lattice with its competing  $J1$ - $J2$  superexchange pathways. The significance of this finding is that this generic frustration will render the spin-orbital degrees of freedom to be extremely soft, opening up the possibility that they turn into strongly fluctuating degrees of freedom—a desired property when one considers pnictide physics.

We argued that the orthorhombic transition in half-filled pnictides and the associated anomalies in transport properties can be related to orbital order. When the parameters are tuned away from the frustration regime the main tendency of the system is to antiferro-orbital ordering, which is the usual situation for antiferromagnets. An important result is that in the regime of relevance to the pnictides where the frustrations dominate we find phases that are at the same time  $(\pi, 0)$  magnets and forms of orbital order that are compatible with orthorhombic lattice distortions (Figs. 4 and 5). Besides the literal ferro-orbital-ordered state [Fig. 5(a)], we find also a  $(\pi, 0)$  or tweed orbital order [Fig. 5(b)]. This appears to be the more natural possibility in the insulating limit, and if the weak superlattice reflections associated with this state would be observed this could be considered as a strong support for the literalness of the strong-coupling limit. Surely, the effects of itinerancy are expected to modify the picture substantially. Propagating fermions are expected to stabilize ferro-orbital orders,<sup>46,47</sup> which enhances the spatial anisotropy of the spin-spin interactions further.<sup>26</sup>

Among the observable consequences of this orbital physics is its impact of the spin fluctuations. We conclude the

paper with an analysis of the spin waves in the orbital-ordered phases, coming to the conclusion that also the spin sector is quite frustrated, indicating that the quantum spin fluctuations should be quite strong, and offering a rationale for a strong reduction in the order parameter.

Thus we have forwarded the hypothesis that the undoped iron pnictides are controlled by a very similar spin-charge-orbital physics as found in ruthenates and manganites. To develop a more quantitative theoretical expectation is less straightforward, and as it is certainly beyond standard LDA and LDA+ $U$  approaches will require investigations of correlated electron models such as we have derived here,<sup>48,49</sup> taking note of the fact that the pnictides most likely belong to the border line cases where the Hubbard  $U$  is neither small nor large compared to the bandwidth.<sup>50</sup>

## ACKNOWLEDGMENTS

The authors would like to acknowledge useful discussions with G. Giovannetti, J. Moore, and G.A. Sawatzky. This work was financially supported by *Nanoned*, a nanotechnology program of the Dutch Ministry of Economic Affairs and by the Nederlandse Organisatie voor Wetenschappelijk Onderzoek (NWO) and the Stichting voor Fundamenteel Onderzoek der Materie (FOM).

## APPENDIX A: EFFECTIVE INTERACTION AMPLITUDES

By acting with the hopping operator  $\mathcal{H}_i$  (2) on all states in the ground-state sector and calculating the overlap of the resulting states projected on the different intermediate states, we find the effective interaction amplitudes. For the high-spin intermediate state ( $n=1$ ) we find by projecting on the intermediate  ${}^4A_2$  multiplet,

$$\begin{aligned}
 f_{zz}^{(1)} &= \frac{4t_{ab}^2 - 2(t_{aa}^2 + t_{bb}^2)}{\epsilon({}^4A_2)}, \\
 f_{+-}^{(1)} &= -\frac{4t_{aa}t_{bb}}{\epsilon({}^4A_2)}, \\
 f_{++}^{(1)} &= -\frac{4t_{ab}^2}{\epsilon({}^4A_2)}, \\
 f_{zx}^{(1)} &= \frac{4t_{ab}(t_{bb} - t_{aa})}{\epsilon({}^4A_2)}, \\
 f_z^{(1)} &= \frac{t_{bc}^2 - t_{ac}^2}{\epsilon({}^4A_2) + \Delta}, \\
 f_x^{(1)} &= -\frac{2t_{ac}t_{bc}}{\epsilon({}^4A_2) + \Delta}, \\
 f_0^{(1)} &= \frac{1}{2} \frac{2t_{ab}^2 + t_{aa}^2 + t_{bb}^2}{\epsilon({}^4A_2)} + \frac{t_{ac}^2 + t_{bc}^2}{\epsilon({}^4A_2) + \Delta}, \quad (A1)
 \end{aligned}$$

where the hopping matrix elements have to be specified for a particular bond. Likewise, we find by projections on the intermediate low-spin states ( $n=2$ ),

$$\begin{aligned}
f_{zz}^{(2)} &= \frac{1}{2}[2t_{ab}^2 - (t_{aa}^2 + t_{bb}^2)] \left[ \frac{4}{\epsilon^2(E)} - \frac{3}{\epsilon^2(T_1)} - \frac{3}{\epsilon^2(T_2)} \right], \\
f_{+-}^{(2)} &= \frac{2t_{aa}t_{bb}}{\epsilon^2(E)} + 3t_{ab}^2 \left( \frac{1}{\epsilon^2(T_1)} - \frac{1}{\epsilon^2(T_2)} \right), \\
f_{++}^{(2)} &= \frac{2t_{ab}^2}{\epsilon^2(E)} + 3t_{aa}t_{bb} \left( \frac{1}{\epsilon^2(T_1)} - \frac{1}{\epsilon^2(T_2)} \right), \\
f_{zx}^{(2)} &= t_{ab}(t_{bb} - t_{aa}) \left( \frac{1}{\epsilon^2(E)} + \frac{3}{\epsilon^2(T_2)} \right), \\
f_z^{(2)} &= \frac{1}{2}(t_{bc}^2 - t_{ac}^2) \left( \frac{4}{\epsilon^2(E) + \Delta} + \frac{3}{\epsilon^2(T_1) + \Delta} + \frac{3}{\epsilon^2(T_2) + \Delta} \right. \\
&\quad \left. - \frac{3(1-v_-^2)}{\epsilon^2(T_1^\Delta)} - \frac{3(1-v_+^2)}{\epsilon^2(T_2^\Delta)} \right), \\
f_x^{(2)} &= \frac{3}{2}t_{ab}(t_{aa} + t_{bb}) \left( \frac{1}{\epsilon^2(E)} + \frac{1}{\epsilon^2(T_1)} \right) + t_{ac}t_{bc} \left( \frac{2}{\epsilon^2(E) + \Delta} \right. \\
&\quad \left. + \frac{3}{\epsilon^2(T_1) + \Delta} - \frac{3}{\epsilon^2(T_2) + \Delta} + \frac{3(1-v_-^2)}{\epsilon^2(T_1^\Delta)} + \frac{3(1-v_+^2)}{\epsilon^2(T_2^\Delta)} \right), \\
f_0^{(2)} &= \frac{1}{8}(2t_{ab}^2 + t_{aa}^2 + t_{bb}^2) \times \left( \frac{4}{\epsilon^2(E)} + \frac{3}{\epsilon^2(T_1)} + \frac{3}{\epsilon^2(T_2)} \right) \\
&\quad + \frac{1}{2}(t_{ac}^2 + t_{bc}^2) \left( \frac{4}{\epsilon^2(E) + \Delta} + \frac{3}{\epsilon^2(T_1) + \Delta} + \frac{3}{\epsilon^2(T_2) + \Delta} \right. \\
&\quad \left. + \frac{3(1-v_-^2)}{\epsilon^2(T_1^\Delta)} + \frac{3(1-v_+^2)}{\epsilon^2(T_2^\Delta)} \right) \\
&\quad + 3t_{cc}^2 \left( \frac{1-v_-^2}{\epsilon^2(T_1^\Delta) + \Delta} + \frac{1-v_+^2}{\epsilon^2(T_2^\Delta) + \Delta} \right). \tag{A2}
\end{aligned}$$

The terms bilinear in the pseudospin operators result solely from hopping processes involving the  $|a\rangle$  and  $|b\rangle$  orbitals only. The hoppings between the  $|c\rangle := |xy\rangle$  orbitals enter only as a positive constant in  $Q^{(2)}$  leading to a conventional antiferromagnetic superexchange contribution. Interestingly, the coupling between the  $|c\rangle$  and  $|a\rangle, |b\rangle$  orbitals results in magnetic field terms for the orbital pseudospins.

## APPENDIX B: HOPPING MATRIX ELEMENTS

For a given As-Fe bond with direction cosines  $l, m, n$ , the  $p$  to  $t_{2g}$  hoppings are given by<sup>32</sup>

$$\begin{aligned}
t_{x,zx} &= n[\sqrt{3}l^2(pd\sigma) + (1-2l^2)(pd\pi)], \\
t_{x,yz} &= lmn[\sqrt{3}(pd\sigma) - 2(pd\pi)], \\
t_{x,xy} &= m[\sqrt{3}l^2(pd\sigma) + (1-2l^2)(pd\pi)], \\
t_{y,zx} &= t_{x,yz} = t_{z,xy},
\end{aligned}$$

$$\begin{aligned}
t_{y,yz} &= n[\sqrt{3}m^2(pd\sigma) + (1-2m^2)(pd\pi)], \\
t_{y,xy} &= l[\sqrt{3}m^2(pd\sigma) + (1-2m^2)(pd\pi)], \\
t_{z,zx} &= l[\sqrt{3}n^2(pd\sigma) + (1-2n^2)(pd\pi)], \\
t_{z,yz} &= m[\sqrt{3}n^2(pd\sigma) + (1-2n^2)(pd\pi)]. \tag{B1}
\end{aligned}$$

Using direction cosines  $(l, m, n)$  ( $l^2 + m^2 + n^2 = 1$ ), with  $|l| = |m|$  resulting from the orthorhombic symmetry, we find that only the following hopping-matrix elements are nonzero,

$$\begin{aligned}
t_{aa}^x &= t_{bb}^y =: t_1, \\
t_{bb}^x &= t_{aa}^y =: t_2, \\
t_{aa}^d &= t_{bb}^d =: t_3, \\
t_{ab}^{d-} &= -t_{ab}^{d+} =: t_4, \\
t_{cc}^x &= t_{cc}^y =: t_5, \\
t_{cc}^d &=: t_6, \\
t_{ac}^x &= t_{bc}^y =: t_7. \tag{B2}
\end{aligned}$$

These hopping matrix elements which are shown schematically in Fig. 2 can be parametrized by the lattice parameter  $\lambda = |n/l|$  and the ratio  $\gamma = (pd\pi)/(pd\sigma)$  as

$$\begin{aligned}
\frac{t_1}{t} &= -2(B^2 - A^2 - C^2), \\
\frac{t_2}{t} &= -2(B^2 - A^2 + C^2), \\
\frac{t_3}{t} &= -(B^2 + A^2 - C^2), \\
\frac{t_4}{t} &= 2AB - C^2, \\
\frac{t_5}{t} &= 2A^2, \\
\frac{t_6}{t} &= 2\left(\frac{B}{\lambda}\right)^2 - A^2, \\
\frac{t_7}{t} &= 2\left(AC + \frac{AB}{\lambda} - \frac{B^2}{\lambda}\right), \tag{B3}
\end{aligned}$$

where we have introduced the overall energy scale  $t = (pd\sigma)^2 / \Delta_{pd}$  and defined for abbreviation

$$A = \frac{\lambda(\sqrt{3} - 2\gamma)}{\sqrt{2 + \lambda^2}},$$

$$B = \frac{\lambda(\sqrt{3} + \lambda^2\gamma)}{\sqrt{2 + \lambda^2\gamma}},$$

$$C = \frac{\sqrt{3}\lambda^2 + (2 - \lambda^2)\gamma}{\sqrt{2 + \lambda^2\gamma}}. \quad (\text{B4})$$

### APPENDIX C: ORBITAL PART OF THE HAMILTONIAN

For the nearest-neighbor bonds along  $\hat{x}$  and  $\hat{y}$  the orbital operators in the spin-orbital Hamiltonian are given by

$$\hat{\Omega}_{x,y} = \frac{1}{2}(\alpha_1^2 + \alpha_2^2)(1 + 2\eta r_1 - \eta r_3)\hat{T}_i^z\hat{T}_j^z + \alpha_1\alpha_2(1 + 2\eta r_1 + \eta r_3)\hat{T}_i^x\hat{T}_j^x + \alpha_1\alpha_2(1 + 2\eta r_1 - \eta r_3)\hat{T}_i^y\hat{T}_j^y \mp \frac{1}{12}\alpha_7^2(7\tilde{r}_2 + 3\tilde{r}_3 - 2\tilde{r}_1 - 3g_1)(\hat{T}_i^z + \hat{T}_j^z) + \frac{1}{8}(\alpha_1^2 + \alpha_2^2)(1 - 2\eta r_1 - \eta r_3) + \frac{1}{12}\alpha_7^2(7\tilde{r}_2 + 3\tilde{r}_3 - 2\tilde{r}_1 + 3g_1) + \frac{1}{2}\alpha_5^2g_2, \quad (\text{C1})$$

$$\hat{\Gamma}_{x,y} = \frac{1}{2}(\alpha_1^2 + \alpha_2^2)\eta(r_1 + r_3)\hat{T}_i^z\hat{T}_j^z + \alpha_1\alpha_2\eta(r_1 - r_3)\hat{T}_i^x\hat{T}_j^x + \alpha_1\alpha_2\eta(r_1 + r_3)\hat{T}_i^y\hat{T}_j^y - \frac{1}{8}(\alpha_1^2 + \alpha_2^2)(2 + \eta r_1 - \eta r_3) - \frac{1}{12}\alpha_7^2(\tilde{r}_1 + 7\tilde{r}_2 + 3\tilde{r}_3 + 3g_1) - \frac{1}{2}\alpha_5^2g_2, \quad (\text{C2})$$

where we have defined  $\tilde{r}_1 = 1/(1 - 3\eta + \delta)$ ,  $\tilde{r}_2 = \tilde{r}_1|_{\eta=0}$ ,  $\tilde{r}_3 = 1/(1 + 2\eta + \delta)$ , and  $r_i = \tilde{r}_i|_{\delta=0}$  and introduced the functions

$$g_1 = \frac{1 + \eta + \delta}{1 + 2\eta - \delta^2}, \quad (\text{C3})$$

$$g_2 = \frac{1 + \eta + 2\delta}{1 + 2\eta(1 + \delta) + 2\delta}. \quad (\text{C4})$$

Likewise, for the bonds along the  $\hat{x} \pm \hat{y}$  diagonals we obtain

$$\hat{\Omega}_{d\pm} = (\alpha_3^2 - \alpha_4^2)(1 + 2\eta r_1 - \eta r_3) \times \hat{T}_i^z\hat{T}_j^z + (\alpha_3^2 + \alpha_4^2)(1 + 2\eta r_1 + \eta r_3)\hat{T}_i^x\hat{T}_j^x + (\alpha_3^2 - \alpha_4^2) \times (1 + 2\eta r_1 - \eta r_3)\hat{T}_i^y\hat{T}_j^y \mp \alpha_3\alpha_4(\hat{T}_i^x + \hat{T}_j^x) + \frac{1}{4}(\alpha_3^2 + \alpha_4^2) \times (1 - 2\eta r_1 - \eta r_3) + \frac{1}{2}\alpha_6^2g_2, \quad (\text{C5})$$

$$\hat{\Gamma}_{d\pm} = (\alpha_3^2 - \alpha_4^2)\eta(r_1 + r_3)\hat{T}_i^z\hat{T}_j^z + (\alpha_3^2 + \alpha_4^2)\eta(r_1 - r_3)\hat{T}_i^x\hat{T}_j^x + (\alpha_3^2 - \alpha_4^2)\eta(r_1 + r_3)\hat{T}_i^y\hat{T}_j^y - \frac{1}{4}(\alpha_3^2 + \alpha_4^2)(2 + \eta r_1 - \eta r_3) - \frac{1}{2}\alpha_6^2g_2. \quad (\text{C6})$$

- <sup>1</sup>Y. Kamihara, T. Watanabe, M. Hirano, and H. Hosono, *J. Am. Chem. Soc.* **130**, 3296 (2008).  
<sup>2</sup>H. Takahashi, K. Igawa, A. Kazunobu, Y. Kamihara, M. Hirano, and H. Hosono, *Nature (London)* **453**, 376 (2008).  
<sup>3</sup>Z.-A. Ren, J. Yang, W. Lu, W. Yi, G.-C. Che, X.-L. Dong, L.-L. Sun, and Z.-X. Zhao, *Mater. Res. Innovations* **12**, 105 (2008).  
<sup>4</sup>X. H. Chen, T. Wu, G. Wu, R. H. Liu, H. Chen, and D. F. Fang, *Nature (London)* **453**, 761 (2008).  
<sup>5</sup>G. F. Chen, Z. Li, D. Wu, G. Li, W. Z. Hu, J. Dong, P. Zheng, J. L. Luo, and N. L. Wang, *Phys. Rev. Lett.* **100**, 247002 (2008).  
<sup>6</sup>M. R. Norman, *Physics* **1**, 21 (2008).  
<sup>7</sup>C. de la Cruz *et al.*, *Nature (London)* **453**, 899 (2008).  
<sup>8</sup>M. A. McGuire *et al.*, *Phys. Rev. B* **78**, 094517 (2008).  
<sup>9</sup>A. I. Goldman, D. N. Argyriou, B. Ouladdiaf, T. Chatterji, A. Kreyssig, S. Nandi, N. Ni, S. L. Budko, P. C. Canfield, and R. J. McQueeney, *Phys. Rev. B* **78**, 100506(R) (2008).  
<sup>10</sup>C. Fang, H. Yao, W. F. Tsai, J. P. Hu, and S. A. Kivelson, *Phys. Rev. B* **77**, 224509 (2008).  
<sup>11</sup>C. Xu, M. Muller, and S. Sachdev, *Phys. Rev. B* **78**, 020501(R) (2008).  
<sup>12</sup>I. I. Mazin and M. D. Johannes, arXiv:08073737 (unpublished).  
<sup>13</sup>A. J. Millis, P. B. Littlewood, and B. I. Shraiman, *Phys. Rev. Lett.* **74**, 5144 (1995).

- <sup>14</sup>(a) K. Kuroki, S. Onari, R. Arita, H. Usui, Y. Tanaka, H. Kon-tani, and H. Aoki, *Phys. Rev. Lett.* **101**, 087004 (2008); (b) V. Cvetkovic and Z. Tesanovic, arXiv:0804.4678 (unpublished); (c) J. Wu, P. Phillips, and A. H. Castro Neto, *Phys. Rev. Lett.* **101**, 126401 (2008); (d) M. Daghofer, A. Moreo, J. A. Riera, E. Ar-rigoni, D. J. Scalapino, and E. Dagotto, *ibid.* **101**, 237004 (2008); (e) A. Moreo, M. Daghofer, J. A. Riera, and E. Dagotto, arXiv:0901.3544 (unpublished).  
<sup>15</sup>K. I. Kugel and D. I. Khomskii, *Sov. Phys. Usp.* **136**, 621 (1982).  
<sup>16</sup>J. van den Brink and D. Khomskii, *Phys. Rev. B* **63**, 140416(R) (2001).  
<sup>17</sup>J. van den Brink and D. Khomskii, *Phys. Rev. Lett.* **82**, 1016 (1999).  
<sup>18</sup>J. van den Brink, G. Khaliullin, and D. Khomskii, *Phys. Rev. Lett.* **83**, 5118 (1999).  
<sup>19</sup>J. Dho, E. O. Chi, W. S. Kim, N. H. Hur, and Y. N. Choi, *Phys. Rev. B* **65**, 132414 (2002).  
<sup>20</sup>T. Akimoto, Y. Maruyama, Y. Moritomo, A. Nakamura, K. Hirota, K. Ohoyama, and M. Ohashi, *Phys. Rev. B* **57**, R5594 (1998).  
<sup>21</sup>H. Kawano, R. Kajimoto, H. Yoshizawa, Y. Tomioka, H. Kuwahara, and Y. Tokura, *Phys. Rev. Lett.* **78**, 4253 (1997).

- <sup>22</sup>X. N. Lin, Z. X. Zhou, V. Durairaj, P. Schlottmann, and G. Cao, Phys. Rev. Lett. **95**, 017203 (2005).
- <sup>23</sup>M. Cuoco, F. Forte, and C. Noce, Phys. Rev. B **73**, 094428 (2006).
- <sup>24</sup>S. Lee *et al.*, Nature Mater. **5**, 471 (2006).
- <sup>25</sup>J. van den Brink, Nature Mater. **5**, 427 (2006).
- <sup>26</sup>M. J. Han, Q. Yin, W. E. Pickett, and S. Y. Savrasov, arXiv:08110034 (unpublished).
- <sup>27</sup>G. Giovannetti, S. Kumar, and J. van den Brink, Physica B **403**, 3653 (2008).
- <sup>28</sup>A. M. Oleś, G. Khaliullin, P. Horsch, and L. F. Feiner, Phys. Rev. B **72**, 214431 (2005).
- <sup>29</sup>A. M. Oleś, P. Horsch, and G. Khaliullin, Phys. Rev. B **75**, 184434 (2007).
- <sup>30</sup>P. Horsch, A. M. Oleś, L. F. Feiner, and G. Khaliullin, Phys. Rev. Lett. **100**, 167205 (2008).
- <sup>31</sup>A. M. Oleś, Phys. Rev. B **28**, 327 (1983).
- <sup>32</sup>J. C. Slater and G. F. Koster, Phys. Rev. **94**, 1498 (1954).
- <sup>33</sup>S. Raghu, X.-L. Qi, C.-X. Liu, D. J. Scalapino, and S.-C. Zhang, Phys. Rev. B **77**, 220503(R) (2008).
- <sup>34</sup>C. Cao, P. J. Hirschfeld, and H.-P. Cheng, Phys. Rev. B **77**, 220506(R) (2008).
- <sup>35</sup>Y. Murakami, H. Kawada, H. Kawata, M. Tanaka, T. Arima, Y. Moritomo, and Y. Tokura, Phys. Rev. Lett. **80**, 1932 (1998).
- <sup>36</sup>I. S. Elfimov, V. I. Anisimov, and G. A. Sawatzky, Phys. Rev. Lett. **82**, 4264 (1999).
- <sup>37</sup>P. Benedetti, J. van den Brink, E. Pavarini, A. Vigliante, and P. Wochner, Phys. Rev. B **63**, 060408(R) (2001).
- <sup>38</sup>Y. Joly, J. E. Lorenzo, E. Nazarenko, J.-L. Hodeau, D. Mannix, and C. Marin, Phys. Rev. B **78**, 134110 (2008).
- <sup>39</sup>Q. Si and E. Abrahams, Phys. Rev. Lett. **101**, 076401 (2008).
- <sup>40</sup>D.-X. Yao and E. W. Carlson, Phys. Rev. B **78**, 052507 (2008).
- <sup>41</sup>J. Zhao *et al.*, Phys. Rev. Lett. **101**, 167203 (2008).
- <sup>42</sup>F. Krüger and S. Scheidl, Phys. Rev. B **67**, 134512 (2003).
- <sup>43</sup>K. I. Kugel and D. I. Khomskii, Sov. Phys. Usp. **25**, 231 (1982).
- <sup>44</sup>L. F. Feiner, A. M. Oleś, and J. Zaanen, Phys. Rev. Lett. **78**, 2799 (1997).
- <sup>45</sup>A. M. Oleś, L. F. Feiner, and J. Zaanen, Phys. Rev. B **61**, 6257 (2000).
- <sup>46</sup>K. I. Kugel, A. L. Rakhmanov, A. O. Sboychakov, and D. I. Khomskii Phys. Rev. B **78**, 155113 (2008).
- <sup>47</sup>S. Kumar, A. P. Kampf, and P. Majumdar, Phys. Rev. Lett. **97**, 176403 (2006).
- <sup>48</sup>V. I. Anisimov, J. Zaanen, and O. K. Andersen, Phys. Rev. B **44**, 943 (1991).
- <sup>49</sup>A. I. Liechtenstein, V. I. Anisimov, and J. Zaanen, Phys. Rev. B **52**, R5467 (1995).
- <sup>50</sup>G. A. Sawatzky, I. S. Elfimov, J. van den Brink, and J. Zaanen, arXiv:08081390 (unpublished).